Protein Phosphatase Biosensor for the Detection of Cyanotoxins Associated with Algal Bloom

UNIVERSITY *of the*
WESTERN CAPE

BY

NONTLE CATHERINE MNIKI

A thesis submitted in partial fulfilment of the requirements for the degree of

Magister Nanoscience in the Department of Chemistry, University of the

Western Cape.

Supervisor

Professor Priscilla G.L. Baker

November 2013

ABSTRACT

The toxicity of microcystin is associated with the inhibition of serine/threonine protein phosphatases 1 and 2A, which can lead to hepatocyte necrosis and haemorrhage. Analysis of microcystin is most commonly carried out using reversed-phase high performance liquid chromatographic methods (HPLC) combined with ultra-violet (UV) detection .The ability of these techniques to identify unknown microcystin in environmental samples is also restricted by the lack of standard reference materials for the toxins. Highly specific recognition molecules such as antibodies and molecularly imprinted polymers (MIPs) have been employed in the pre-concentration of trace levels of microcystin from water and show great potential for the clean-up of complex samples for subsequent analysis. New biosensor technologies are also becoming available, with sufficient sensitivity and specificity to enable rapid 'on-site' screening without the need for sample processing.

In this work we constructed a Protein phosphatase biosensor for detection of microcystin-LR in aqueous medium, onto polyamic acid/graphene oxide (PAA: GO) composite electrochemically synthesised in our laboratory. The composites were synthesised at three different ratios i.e. 50:50, 80:20 and 20:80 to evaluate the effect of each component in the search to produce highly conductive mediator platforms. The electrochemistries of the three different composites were evaluated using CV and SWV to study interfacial kinetics of the materials as thin films at the glassy carbon electrode. The phosphatase biosensor parameters were evaluated using CV, SWV, EIS and Uv-vis spectroscopy. The affinity binding of the microcystin-LR to protein phosphatase 2A was investigated using electrochemical impedance spectroscopy which is a highly sensitive method for measuring interfacial kinetics of biosensor systems.

KEYWORDS

Protein phosphatase1 and 2a

Polyamic acid

Graphene oxide

Microcystin-LR

Biosensor

Cyanotoxins

Cyclic voltammetry

Uv-vis spectroscopy

Atomic force microscopy

Scanning electron microscopy

Electrochemical impedance spectroscopy

Enzyme linked immunosorbent assay

DECLARATION

I declare that **"Protein phosphatase biosensor for the detection of Cyanotoxins associated with algal bloom"** is my own work, that it has not been submitted before for any degree or assessment in any other university, and that all the sources I have used or quoted have been indicated and acknowledged by means of complete references.

Nontle Catherine Mniki **November 2013**

Signature …… ……

Supervisor: **Prof. Priscilla G.L. Baker**

ACKNOWLEDGEMENT

I would like to thank the all mighty for giving me the strength throughout my studies. I wish to express my deep appreciation for my supervisor Professor Priscilla Baker for her guidance academically, patience and encouraging words, for believing in me from my honours degree till my Masters. I would like to appreciate members of Sensor Lab research group for their input and suggestion throughout my research. I would also like to thank my aunt Sibulelo Mniki for the support and love she has shown me through hard times and good times. She played a role of being a mother to me. I would like to acknowledge my dearest daddy Nceba Mniki for supporting me. Also big thanks to Veronica Shipalana for taking care of my little angel Oyama Katekani Mniki while I was busy with my school work. My sisters Asanda Duda, Namhla Mniki, Yongama Mniki and my brothers Vuyo Mniki, Zusiphe Mniki and Ntinga Mniki for their love and prayers. Last but not least my best friend Remember Shipalana for your advice and support. Finally I would like to acknowledge my financial sponsor Department of Science and Technology (DST) for financial support and University of the Western Cape.

DEDICATION

I dedicated this project to everyone in my family as whole, especial:

My Daughter

Oyama Katekani Mniki

And

My late mother

Nokhaya Nomonde Mbawu

CONFERENCE

Nontle Catherine Mniki, Euodia Hess, Xolani Simelani, Priscilla Baker*; "Protein phosphatase biosensor for the detection of Cyanotoxins associated with algal bloom; 13th international society electrochemistry". (07-11) April 2013. Council for Scientific Industrial Research, international convention centre in Pretoria.

LIST OF ABBREVIATIONS

HABs	Harmful Algal Blooms
MC-LR	Microcystin-LR
HPLC	High performance liquid chromatograph
GC-MS	Gas chromatography mass spectroscopy
ELISA	Enzyme linked immunosorbent assay
LD50	Lethal dose of 50%
PP2a	Protein Phosphatase 2a
SWV	Square wave voltammetry
CV	Cyclic Voltammetry
AFM	Atomic Force Microscopy
SEM	Scanning Electron Microscopy
FTIR	Fourier Transform Infrared Spectroscopy
EIS	Electrochemical impedance spectroscopy
PAA	Polyamic acid
GO	Graphene oxide
PBS	Phosphate buffer solution
PPI	Protein phosphatase inhibitor
WHO	World health organisation

CYN	Cylindrospermopsin
ATP	Adenosine triphosphate
EDTA	Ethylenediaminetetraacetic acid
PMSF	Phenyl methyl sulfonyl fluoride
Ca	Calcium
Mg	Magnesium
EPA	Environmental protection Agency
PMDA	Pyromellitic dianhydride
ODA	Oxydianaline
Cu	Copper
DMSO	Dimethyl sulfoxide
De	Diffusion coefficient
AEBS. HCl	4-(2-Aminoethyl) benzenesulfonyl fluoride hydrochloride
SP	Species

TABLE OF CONTENT

LIST OF FIGURES

LIST OF TABLES

LIST OF SCHEME

CHAPTER 1

The mass occurrence of toxic phytoplankton organisms has a negative impact on water quality and the sustainable development of an aquatic ecosystem. The blooms pose a potential health threat, especially when they occur in drinking and recreational waters. This chapter will give an introduction and literature review on cyanotoxins and their health impact based on the toxicity of cyanotoxins such as microcystin, nodularin etc. Analytical methods will be debated to monitor these cyanotoxins as well as the risk exposure to humans and animal.

1.1 Introduction

Toxic cyanobacteria in South Africa found in municipal, residential water supplies, groundwater and eutrophication of fresh water lakes. Eutrophication is the process of excessive nutrient enrichment of waters that typically results in problems associated with macrophyte, algal or cyanobacteria growth. Practically there are no fresh water lakes in South Africa due to eutrophication. Blooms of cyanobacteria tend to occur repeatedly in the same water, posing a risk of repeated exposure to some human populations, where available water supplies are limited to rivers, artificial lakes behind dams and groundwater (Botha, 2005). The mass occurrence of toxic phytoplankton organisms has a negative impact on water quality and the sustainable development of an aquatic ecosystem. The blooms pose a potential health threat, especially when they occur in drinking and recreational waters.

Cyanobacteria are seasonally occurring in South Africa and the species that cause bloom formation are Microcystis sp, Anabaena sp, Oscillatoria sp, and Cylindrospermopsis sp. They are known to produce cyanotoxins which are particularly problematic in drinking water .The acute health effects of exposure to microcystin-LR has received increasing attention around

the world and has been well documented (Gehringer Michelle M., 2003). Toxic cyanobacterial blooms are a sign of the eutrophication of water resources, a problem common to most of the world's nations. As cyanobacteria have the tendency to produce a wide variety of particularly poisonous toxins, toxic blooms of these organisms pose significant problems for, human and animal health, ecosystem health, costs of water treatment and/or availability of raw potable water supply, recreational use and property values at or near affected waters. The incidence of cyanobacterial blooms and associated problems are often of an intermittent or seasonal nature, while in certain cases climatic conditions support levels of cell development that are disturbing to water resource use for much of the year.

The degree to which rural domestic and agricultural water resources are affected is currently unknown. The problem is no less severe in the southern as opposed to the northern hemisphere but, given the milder climate and warmer conditions, the duration of conditions that sustain algal development are prolonged in southern hemisphere countries. Acute poisoning of humans reported from South America, Africa and Australia. The estimated health risk to humans is via chronic exposure to low levels of cyanotoxins in drinking water supplies. The exposure to cyanobacterial toxins is mainly through fish consumption and blue-green algal products used as food supplements, dermal contact, consumption of animal meat and ingestion of contaminated water.

There were several reports done on animals and human exposures to hepatotoxins. The earliest reported cases on human poisoning by gastro-enteritis from cyanobacteria occurred in Harare and Zimbabwe, children living in an area of the city supplied from a particular water reservoir, developed gastro-enteritis each year at the time when a natural bloom of Microcystin was decaying in the reservoir. Other children in the city with different water

supplies were not affected and no infectious agent was identified (Zilberg, 1966). Exposure through swimming in the water containing toxic blooms may cause ear, eye and skin irritation. There were also reports of the death of wild animals and domestic animals caused by ingestion of water and food contaminated by cyanotoxins. The threat is increasing with the spread of hitherto undetected species, such as Cylindrospermopsis, and the heightened risks posed by mixtures of toxins containing both tumor promotion and carcinogenic elements, such as is the case in mixed blooms of Microcystis and Cylindrospermopsis underpin the cause for additional concern. Until the mid-1980s South Africa was a world-leader in research in the fields of eutrophication, cyanobacterial physiology and eco-physiology and cyanotoxins. South Africa now finds itself at a significant disadvantage in that it possesses very limited intellectual and infrastructural capacity in both the causative field of eutrophication and its symptomology of cyanobacterial development.

Harmful algal bloom (HAB), also known as a red tide, is the proliferation of toxic irritation algae that cause a negative impact to natural resources or public health threats. The reason why these blooms called red tide is that many were composed of dinoflagellates containing red pigments which when present in high densities, colored the water red. However, algal blooms may also be green, yellow, or brown, depending on the type of algae present and their coloring. Most of these blooms were often dominated by cyanobacteria, also known as blue-green algae. These cyanobacteria possess vesicles, which provide buoyance and a mechanism that allows them to control their vertical migration in the water column. During a HAB event, algal toxins can accumulate in predators and organisms higher up the food chain. Toxins may also be present in ambient waters, where wave action or human activities can create aerosols containing toxins and cellular wreckage (Figueiredoa et al, 2004).

Animals, including humans, can expose to HAB-related toxins when they eat contaminated seafood, have contact with contaminated water, or inhale contaminated aerosols. Most harmful algal blooms are harmful by virtue of their sheer biomass, whereas others are associated with algal blooms capable of producing toxins. However, not all algal blooms are toxic some are non-toxic. Microalgae that multiply out of control cause major ecological impacts such as the displacement of indigenous species, habitat alteration, or oxygen depletion in the bottom waters. Some HABs are not algae at all, but are small animal-like protists that obtain their nutrition by grazing not by photosynthesis (Landsberg, 2002).

Microcystins are cyclic peptides, containing seven amino acids. Microcystins are the most abundant of the cyanotoxins, comprising over 80 Analogs (Jussi Meriluotoa et al, 1998). They consist of five invariant amino acids namely, D-analine (position 1), Dimethyl aspartic acid (position 3), Adda (position 5), D-glutamic acid (position 6) and N-methyldehydroanine (position 7). With two variant amino acids at positions 2 and 4 which are normally L-amino acids .They are relatively polar molecules due to the presence of free carboxylic acids in their structures and the frequent presence of argine with a free side chain in positions 2 and 4 (Falconer et al, 2005). Evidence of *M.aeruginosa* in dead ducks, revealed that Shin-ike pond Hyogo Prefecture had become eutrophic from the entry of untreated sewage following an earthquake in January 1995, when a sewage treatment plant was damaged. Later that same year September, some 20 ducks died at the site of Oo–ike pond, also due to toxic cyanobacteria bloom, but no unusual bird deaths were reported from that site.

Water samples were collected from both ponds. Necropsy of one of the affected ducks showed a liver that was necrotic. Preliminary toxicity testing with sonicated cell suspensions using a mouse bioassay resulted in unspecified signs of Microcystis toxicity and death within

two hours from the Shin–ike pond in hyogo material, whereas that from Oo–ike pond hyogo did not produce signs of acute toxicity. Quantification of microcystins by HPLC revealed that Shin–ike pond lyophilised bloom material contained 318μg/g MC–RR, and 161μg/g MC–LR. Oo–ike pond cyanobacteria contained 29μg/g MC–RR and no detectable MC–LR (Matsunaga et al. 1999). While tissues from affected birds were not analysed for microcystins, the combination of necropsy, bioassay and microcystin quantification, along with differential findings between the suspect pond and a nearby "control" site provide strong support to the probable/presumptive diagnosis of acute microcystin intoxication in this case

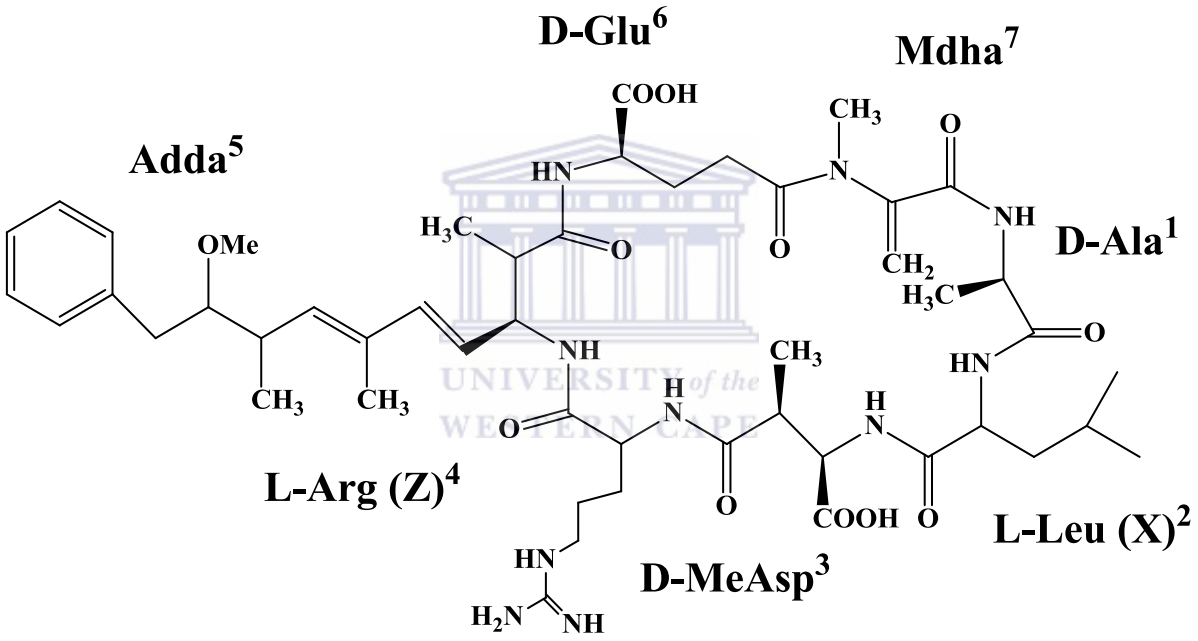

Figure 1: Structure of microcystins

The analytical methods used for monitoring microcystins and nodularin

Enzyme-linked immunoasorbent assay (ELISA), protein phosphatase inhibition assay (PPI) and mouse assay (MA) have been used as screening techniques for microcystins and nodularins. **Mouse assay** is not that widely used anymore because of its many disadvantages, yet it remains a reliable screening method giving results within few hours. Mouse assay was able to differentiate between hepatotoxins and neurotoxins and provided information on the

minimum amount of toxin to kill mouse and compared it with the value of lethal doses of known amounts of toxin.

High performance liquid chromatography (HPLC) method involved lengthy analysis time and methods to concentrate or clean the samples since the detection level are relatively high (Lambert et al, 1994). Therefore, the method is not best for rapid detection of low toxin concentrations which is needed for example in the monitoring of drinking waters. Analysis in laboratories has mainly been based on reversed-phase high-performance liquid chromatographic methods which required expensive equipment and highly qualified personnel due to the high variability of toxin structures. HPLC methods allowed for simultaneous determination of microcystins variants (LR, RR, and YR).

HPLC with photo diode array (PDA) was found to be the most precise method for the detection of hepatotoxins, but was limited by the availability of toxin standards (Mackintosh et al, 1994). HPLC coupled with UV (HPLC-UV) detection was also limited due to the narrow absorption wavelength spectra microcystins (200-300nm) where most variants occurred, while in using HPLC coupled with Mass spectrometer (HPLC-MS), the molecular weight of toxins gave rise to more accurate identification of microcystins.

Enzyme linked immunosorbent assay was coined by Engvall and Perlmann 1971 for non-competitive HetEIA configuration, whereas EIA historically denoted a competitive one (Butler, 2000). Enzyme-linked immunosorbent assays (ELISAs) using polyclonal a (Brooks et al, 1998) or monoclonal (Chu et al, 1990; An et al, 1994) antibodies for microcystins were highly specific, sensitive and quick methods to detect microcystins and nodularin. Kits are commercially available from Strategic Diagnostics Inc., Newark, DE; EnviroLogix Inc., Portland, ME; Wako Chemicals, Osaka, Japan and Abraxis LLC products and are easy to operate. Due to specificity and sensitivity, no tedious sample preparation steps are needed.

Problems in the assay arise from the high structural variation of microcystins since the cross-reactivity of the antibodies with different microcystin variants may be variable and does not always correlate with their toxicity. The technical requirements are not as demanding as with to HPLC, and have proved to be reliable in detecting and monitoring drinking water for microcystins

The protein phosphatase inhibition assay (PPI assay) was developed on the basis of the ability of microcystins and nodularin to inhibit serine–threonine protein phosphatase enzymes. Phosphate inhibition by microcystins and nodularin is determined using ^{32}P radiolabelled substrates, though Phosphatase inhibition assay is sensitive it suffers from one major drawback, that the ^{32}P isotopes has a short half-life approximately 14 days (Chorus,2001). The colorimetric applications (Wayne et al, 1997; Jarkko Rapala et al, 2002) were less expensive and more convenient than the radio isotopic ones. Not all microcystin variants reacted with protein phosphatase enzymes to a similar extent and the assay was sensitive to protein phosphatase inhibitors other than microcystins, such as okadaic acid.

In addition, the cyanobacterial sample itself may contain phosphatase activity that masks the presence of toxins (Sim et al, 1993 and Mudge et al, 1994). PPIA is based on the inhibition of protein phosphatases by microcystins on a molecular level and shows comparable results for microcystin-LR equivalents with HPLC and ELISA. Among those above mentioned methods city of Cape Town uses using the ADDA-Abraxis kit as primary screening test and for quantification for algal toxins in drinking water.

The World Health Organisation (WHO) has proposed a guide value of 1 $\mu g\ l^{-1}$ for the most common microcystin variant, microcystin-LR, in drinking water (WHO, 1997). This is one

reason why sensitive, rapid and simple tests suitable for monitoring purposes are needed. International standardisation of microcystin analysis with HPLC is currently under progress.

1.2 Problem statement and research motivation

Cyanobacteria have been linked to illness in various regions throughout the world, including North and South America, Africa, Australia, Europe, Scandinavia and China. There are no reliable figures for the number of people affected worldwide. The only documented and scientifically proved human deaths due to cyanobacterial toxins have been due to exposure during dialysis. People exposed through drinking-water and recreational-water has required serious hospital care. Based on the eutrophication of water in surface area, organisms like shellfish are found to contain very high concentration of these toxins, since these toxins can accumulate in them without being lethal to the shellfish itself. There have been several reports on consumers of such poisoned organisms including humans and animal, that has been affected. Apart from reports worldwide, as early as 1940, shellfish poisoning have been reported in South Africa (Sapeika, 1958, and Grindley, 1969). Most commonly analysis of microcystins was carried out using reversed-phase high performance liquid chromatographic methods (HPLC) combined with ultra-violet (UV) detection, ELISA, Mouse bioassay and GC-MS detection.

The ability of these techniques to identify unknown microcystins in environmental samples was restricted by the lack of standard reference materials for the toxins. Among all the techniques that have been used, biosensors have emerged as the runner in toxin detection and monitoring in the environment. Biosensors are cost effective compared to HPLC method and electrochemical techniques exhibit low detection limits and high sensitivities. Based on earlier reports based on biosensor screening for microcystins, they detect in the lower μgl^{-1} concentration range and are inexpensive. Biosensors have the added advantage that they are portable and maybe used for on-site and even in situ analysis.

1.3 Aim and objectives

In this work we aim to develop a suitable platform for the immobilisation of protein phosphatase to produce a biosensor for the detection of cyanotoxins associated with algal bloom. The work may be delineated by the following aims and objectives:

(i) Chemical Synthesis of graphene oxide and polyamic acid as the starting materials for the electrochemical synthesis of biosensor platform;

(ii) Electrochemical synthesis of graphene oxide: polyamic acid composites with improved stability and enhanced electrochemical performance;

(iii) Spectro-electrochemical characterization of polyamic acid, graphene oxide and their composites

(iv) Morphological characterization of polyamic acid, graphene oxide and their composites;

(v) Electrochemical interrogation of the novel biosensor performance;

(vi) Electrochemical impedance interrogation of affinity binding of microcystin to Protein phosphatase 2A

(vii) Evaluation of biosensor response parameters such as the limit of the detection and sensitivity of protein phosphatase 2A biosensor towards microcystin-LR;

(viii) Enzyme-linked immunosorbent assay of selected samples for comparison to biosensor performance

1.4. Research framework

The research design is summarised in the diagram in the scheme below:

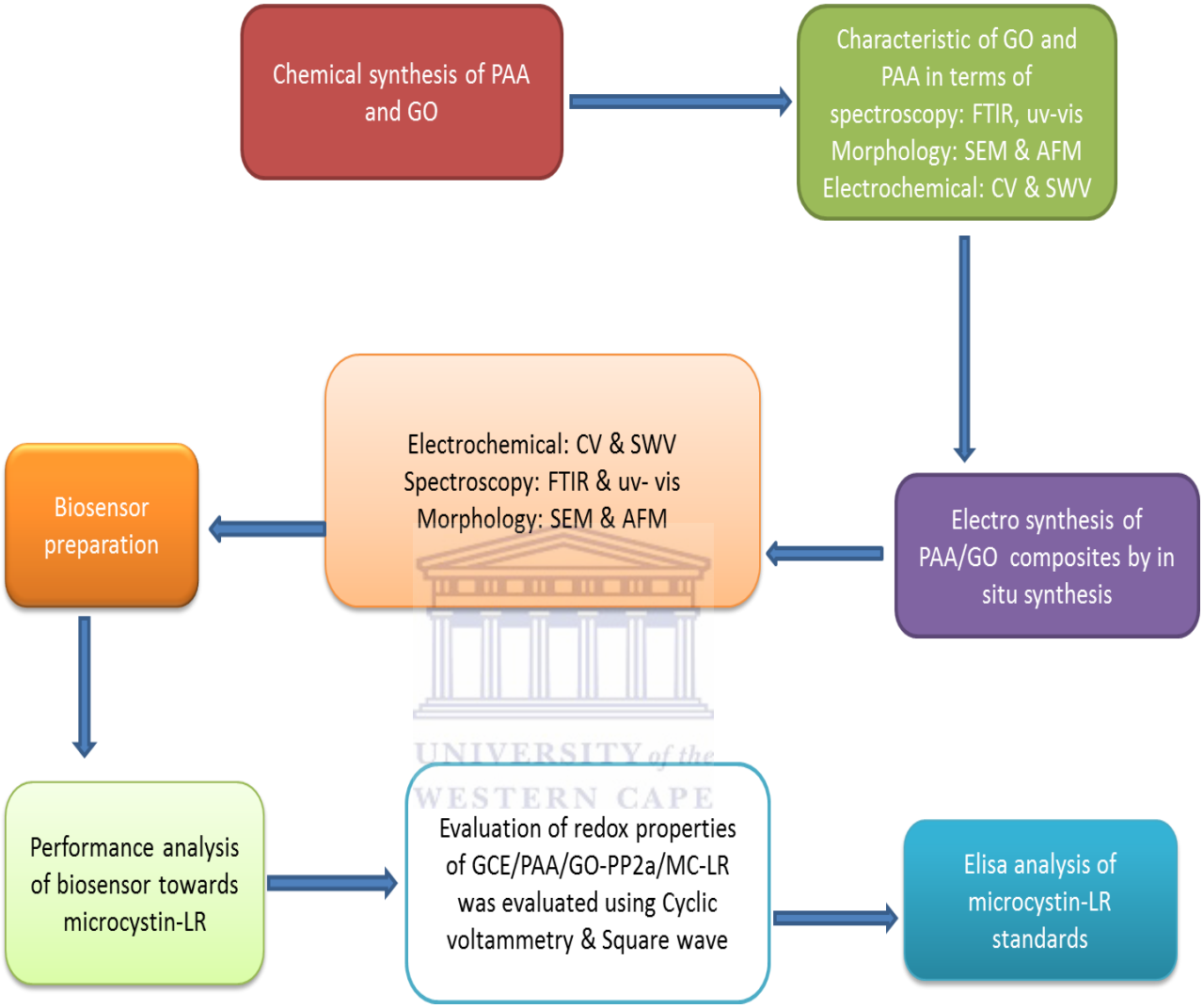

SCHEME: 1 Research framework

Therefore the detection and qualification of the MC-LR in water bodies remains a pressing environmental problem. In this work we will show that a biosensor specifically designed and constructed for detection of microcystin-LR in aqueous environment, yielded promising results which may be extrapolated for on- site portable use.

CHAPTER 2

This chapter will give an introduction to different toxins relevant to water treatment and the construction of a biosensor system will be outlined.

2.1. Cyanobacterial -toxin

Cyanobacteria are microscopic organisms found naturally everywhere such as in lakes, stream or ponds and ocean where they reproduce exponentially to form blooms. Blooming cyanobacteria produce cyanotoxins in concentrations that are poisonous to animals and humans. Cyanotoxins are recognized to have caused the deaths of wild animals, farm livestock, pets, fish and birds in many countries (Botha et al, 2005). The major target organ of most cyanotoxins in mammals is the liver (hepatotoxic). The cyanotoxins are a very diverse group of toxins from both the chemical and toxicology position. They have been arranged based on their toxicological properties such neurotoxins (anatoxin-a, anatoxin-a(s), saxitoxin and neosaxitoxin) microcystins and lipopolysaccharides which are the tumor promoters, lyngbyatoxin A, apysiatoxins and lipopolysaccharides (the dermatotoxins/ irritant toxins; hepatotoxins (microcystins, cylindrospermopsin and nodularin) (Msagati et al, 2006, Monica Campas et al, 2007).

Based on their chemical structure microcystin are the most widespread of all the cyanobacterial hepatotoxins and are produced mainly by cyanobacteria belonging to the genera Microcystins, Anabaena, Planktothrix and Nostoc (Spoof et al, 2003). Microcystin genus is ubiquitous of the genera and produces the most commonly found hepatotoxins, called microcystins. The species M.aeruginosa appears to be the most abundant species producing toxic blooms (Mackintosh et al, 1990).

2.1.1 Cylindrospermopsins

This cyanotoxin was initially isolated from a culture of Cylindrospermopsin raciborskii obtained from a water supply reservoir in tropical northern Australia. The organism was identified as a result of an outbreak of acute hepato-enteritis and renal damage among an Aboriginal population on Palm Island, off the coast of North Queensland (Hawkins et al, 1997; Schembri et al, 2001). Cylindrospermopsins are alkaloids comprised of a tri-cyclic guanidine moiety linked via a hydroxylated bridging carbon (C7) to uracil (Ohtani et al, 1992). The primary toxic effect of parent compound appears to be irreversible protein synthesis inhibition; however there is also evidence for metabolic activation as inhibitors of cylindrospermopsins 450s are able to reduce acute toxicity, CYN-dependent inhibition of glutathione synthesis (Runnegar et al, 1995; Terao et al, 1994).

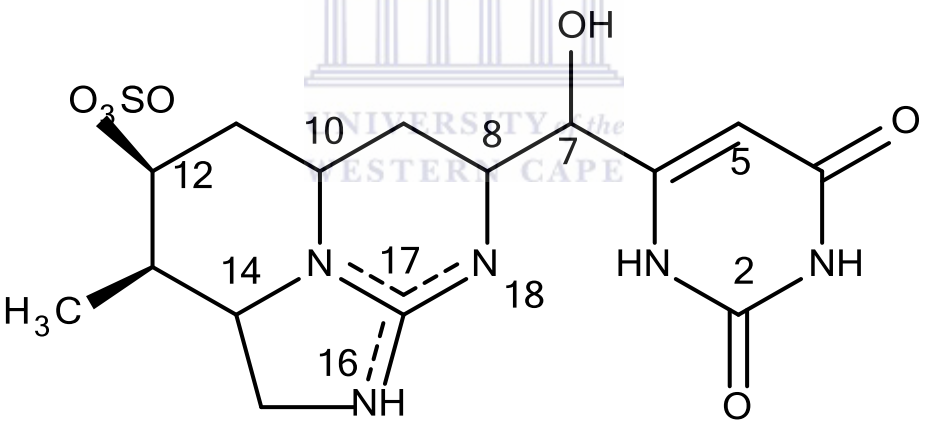

Figure 2: Structure of Cylindrospermopsin

2.1.2 Saxitoxin

Saxitoxins are alkaloids based on a 3, 4, 6,-trialkyl tetrahydropurine skeleton which can be further carbamylated, sulphated or N-sulphocarbamylated to produce a range of 30 analogues (Shizu, 2000). Saxitoxins have an effect or involvement with paralytic shellfish poisoning where shellfish get through toxigenic marine dinoflagellates, which concentrate the toxins and can deliver toxic quantities to consumers of shellfish (Kao, 1993) some which can only found in fresh water cyanobacteria. These toxins are produced in freshwater environment by anabaena circinalis, Cylindrospermopsis raciborskii, and Planktothrix sp (Li et al, 2003; Carmichael et al, 1997). The signs and symptoms of PSP in humans may range from a slight tingling and numbness about the lips to complete paralysis and death from respiratory failure.

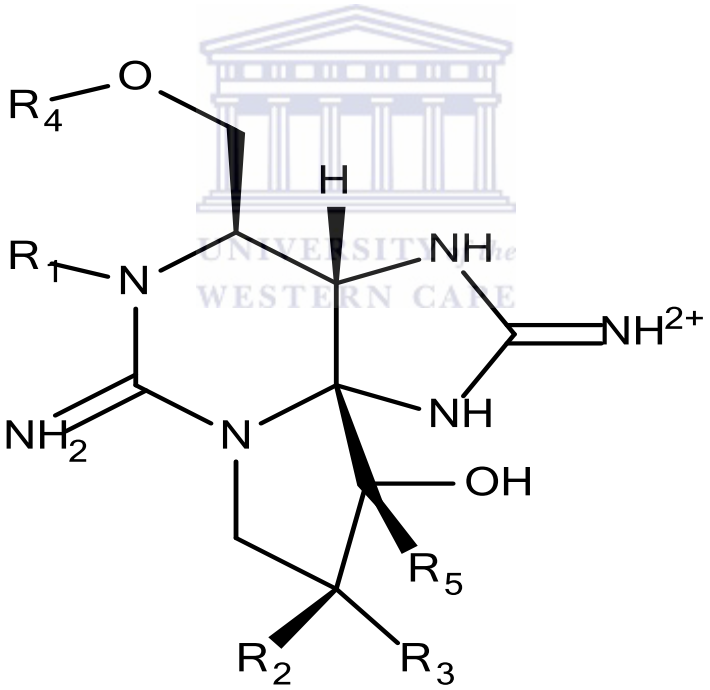

Figure 3: **General structure of saxitoxin**

2.1.3 Nodularin

Nodularin, a cyclic pentapeptide cyanotoxin produced by a cyanobacterium, Nodularia spumigena, was first discovered and characterized in the late 1980s. Nodularin is similar to microcystins in that it contains a unique C20 amino acid, 3-amino-9methoxy-2, 6, 8-trimethyl-10-phenyl-4, 6-decadienoic acid and an Adda (Zhou et al, 2011; Rinehart et al, 1988). The Nodularia spumigena is mostly detected in algal blooms forming from brackish and fresh waters in the universe.

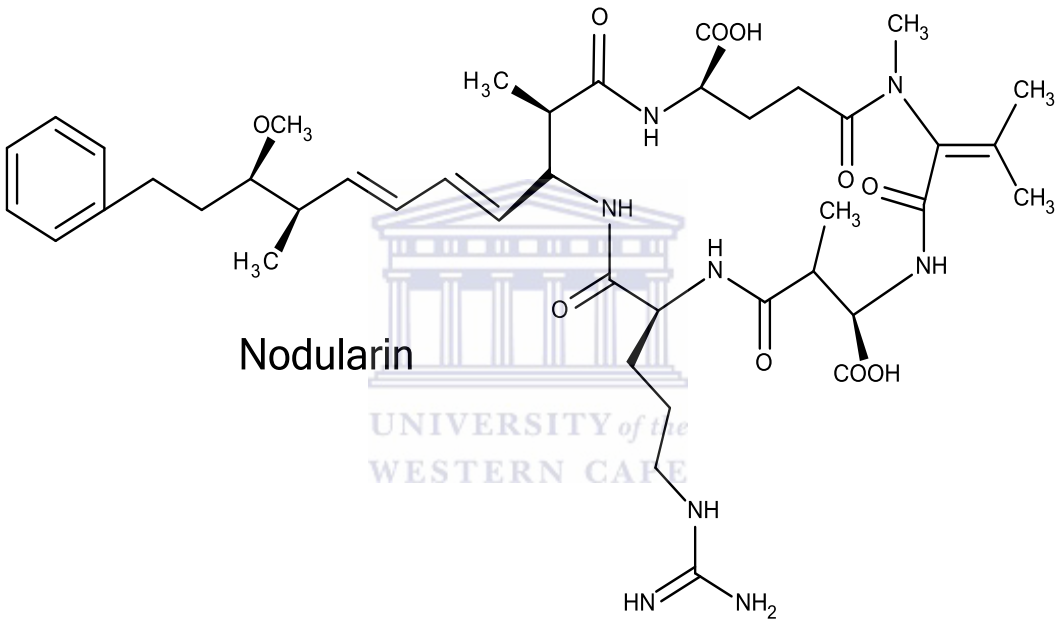

Figure 4: Structure of nodularin

2.1.4 Anatoxin-a

Anatoxin-a(S) is an organophosphate produced by the cyanobacteria Anabaena flos-aquae and anabaena lemmermannii. This toxin blocks acetyl cholinesterase activity in a manner analogous to organophosphate insecticides. It is produced by anabaena flos-aquae, A. planktonic, Aphanizomenon sp, Planktothrix Formosa, and a benthic Oscillatoria sp (Sivonen et al; 1989; Edwards et al, 1992; Skulberg et al, 1992; Bruno et al, 1994, and Bunke-Vogt et al, 1999). These toxins are nicotinic acetylcholine receptor agonists having a LD50 of 200 µg kg-1 (Carmichael 1994). This toxin has not been linked with human poisoning via drinking contaminated water although evidence has been reported in Florida that such risk can happen (Burns 2005). In California reports were released that dog deaths have been attributed to poisoning by these toxins when the animals have licked their coats after swimming (Codd et al, 1992).

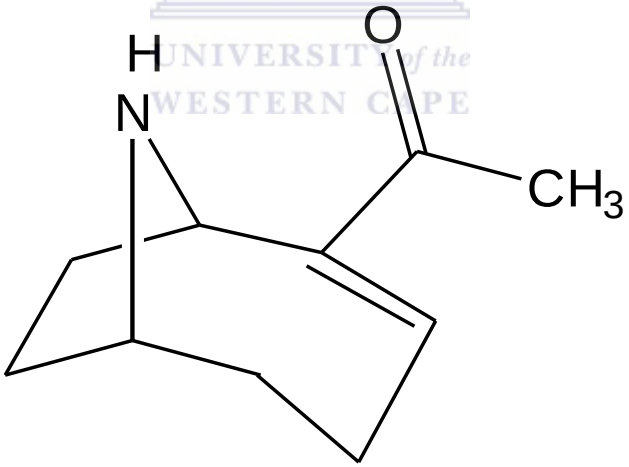

Figure 5: Structure of anatoxin-a

2.1.5 Anatoxin-a(s)

Anatoxin-a(s) is a phosphorylated cyclic N-hydroxyguanine, with a structure and action similar to organophosphate pesticides (Mahmood and Carmichael, 1986; Mahmood and Carmichael, 1987). It is a potent acetyl cholinesterase inhibitor with a LD50 (ip, mouse) of 20µg kg-1. The in vivo toxic effect are similar to those of anatoxin-a, but with the addition of salivation (hence the s) and lacrimation (Matsunaga et al, 1989). There have been no reports to date linking illness in humans to this toxin (Sivonen et al, 1999).

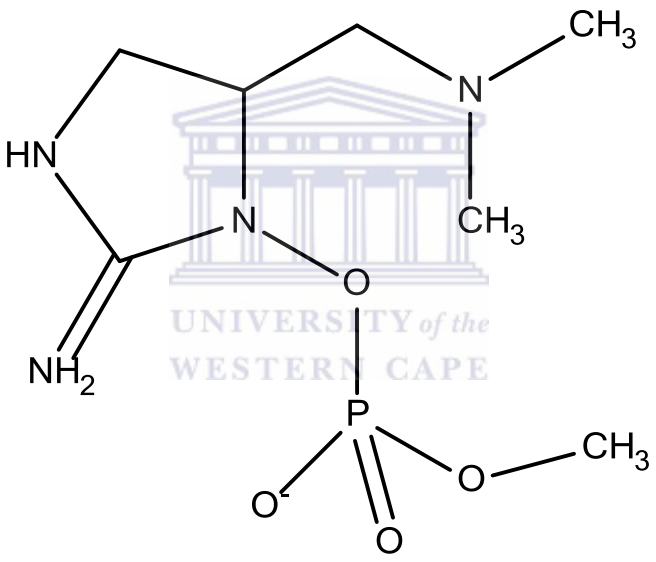

Figure 6: Structure of anatoxin

Environmental impacts include various water quality impacts like increased cyanotoxins levels and lowering of oxygen levels (due to decay of algae and cyanobacteria). Decreased oxygen levels can have a number of other minor water quality effects. Anaerobic conditions allow reduced chemical species (like ammonia and sulphide) present (Chorus, I., and J. Bartram, 1999).The microcystins are cyclic heptapeptides with variable amino acids at 7 different positions. The name microcystin derived from the toxins that were first isolated from Microcystis aeruginosa. The toxicity of microcystins is due to their strong binding to

protein phosphatases, protein phosphatase removes phosphate from protein. Human health concern relates primarily to drinking-water and to recreational water exposure. Some cyanobacteria produce floating "scums" that concentrate cells and any toxins present. So among cyanotoxins there are massive powerful poison known as Neurotoxins, hepatotoxins, cytotoxins and endotoxins they can cause rapid death by respiratory failure.

- **LD50** is an abbreviation of lethal dose of 50%; it is the amount of the substance required usually per body weight to kill 50% of the test population.

Table 1: Comparison of toxicities of biological toxins (Botha A.M et al, 2005)

Toxins	Sources	Lethal doses (LD50)
Saxitoxin	Aphanizomenon flos-aquae	10
Cobra toxin	Anabaena flos-aquae	20
Cobra toxin	Naja naja	20
Nodularin	Nodularia spumigena	30
Microcystin-LR	Microcystis aeruginosa	50
Anatoxin-a	Anabaena flos-aquae	200
Brevetoxin	Karenia brevis (dinoflagellate)	500
Ciguaton	Gambier discus toxicus (dinoflagellate)	0.25
cylindrospermopsins	Clindrospermopsins raciborskii	2100

2.2 Biosensor

A biosensor is an analytical device made up of a combination of specific biological component and electrode transducer which employ bio-molecular recognition as the basis of selective analysis. Interest in the field of bio- analytical chemistry around the use of biosensor continue growing because biosensor offer inexpensive, less complicated, highly sensitivity techniques for detection and analysis, compared to classical methods such as high performance liquid chromatograph (HPLC) methods and enzyme linked immunoassay (ELISA).

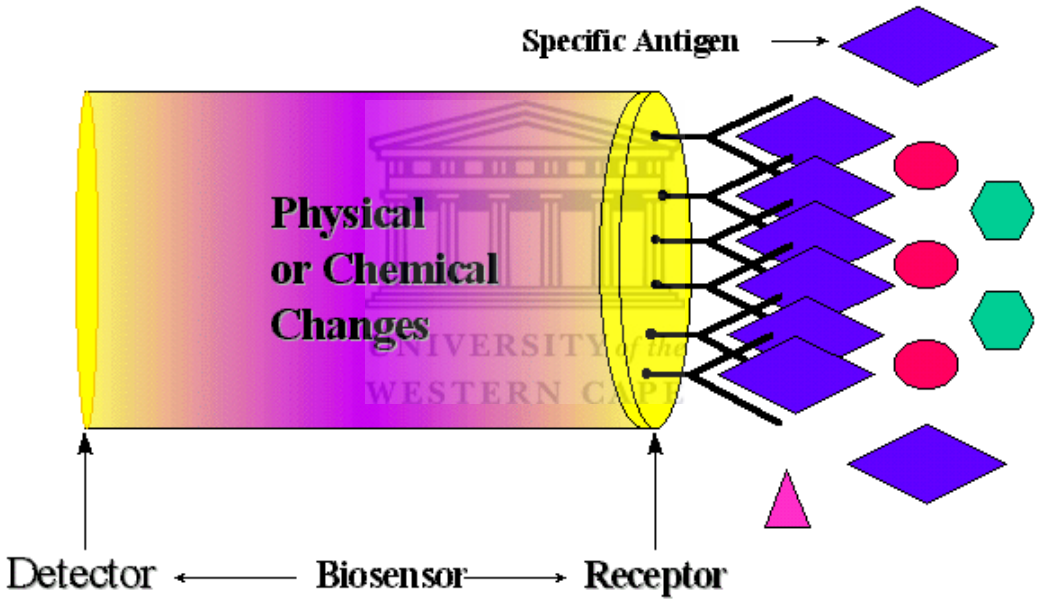

Figure 7: Schematic illustration of a biosensor

(www.tms.org/pubs/journals/JOM/0010/Kumar/Kumar-0010.html)

Biosensors offer the opportunity for use in the analysis of toxins, pollutants, disease markers, genetically modified food, and many other environmental, food, biomedical and explosive detection applications (Zhao et al., 2010; Joseph et al., 2006). Though normally generalized, the bio recognition elements for biosensors are usually enzymes.

In the design of the biosensors employed in this research we used protein phosphatase as the bio-recognition element immobilised at a graphene oxide/polyamic acid thin film layer on glassy carbon electrode to detect cyanotoxins. We focussed on the detection of microcystin-LR in aqueous samples. The biosensor design may be illustrated as follows (scheme 2):

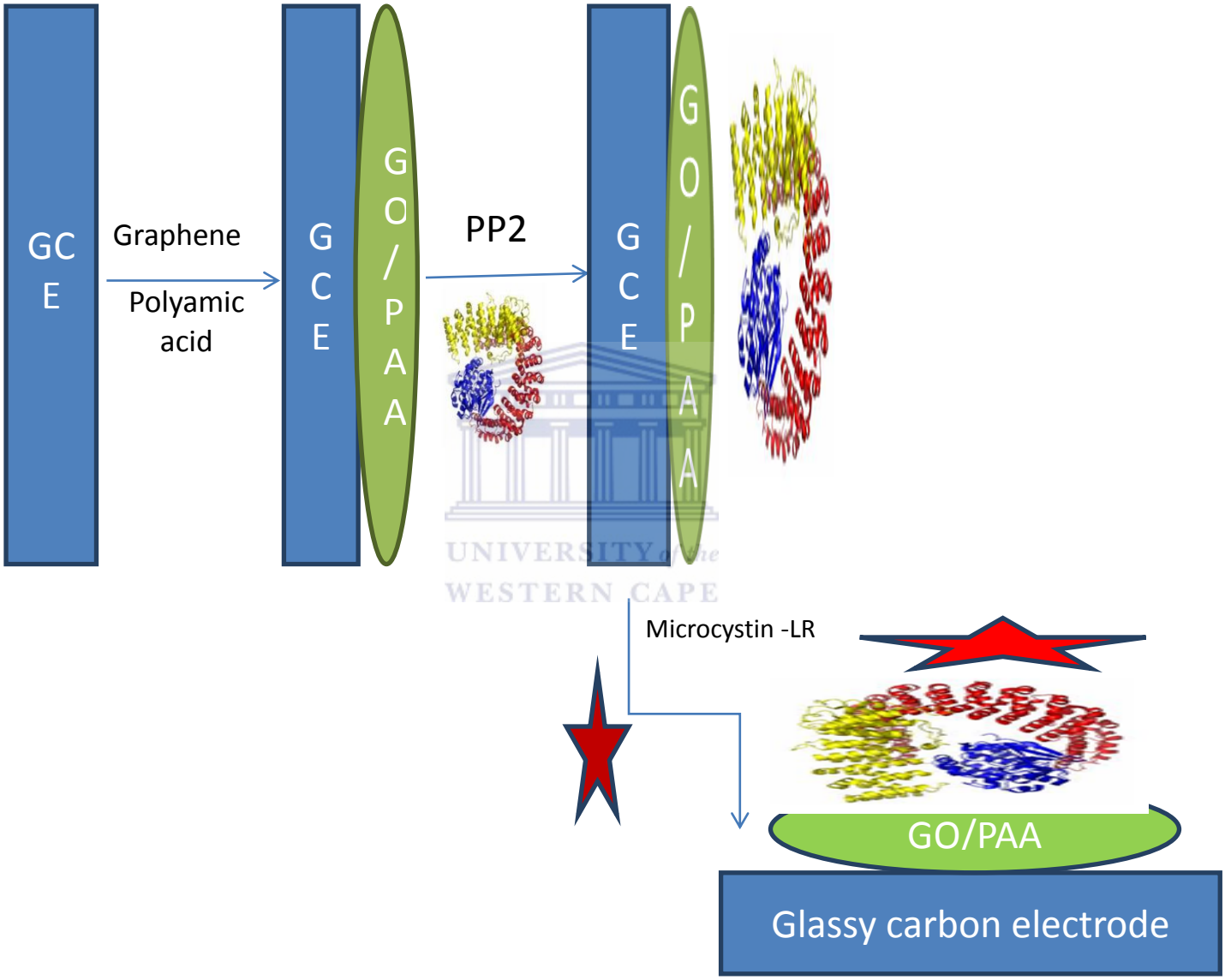

SCHEME: 2 representation of pp2a based biosensor design

2.3 Protein phosphatase

A phosphatase is an enzyme that removes a phosphate group from its substrate by hydrolysing phosphoric acid monoesters into a phosphate ion and a molecule with a free hydroxyl group. Phosphatases play a key role in regulating signal transduction events in eukaryotic cells. Protein kinases transfer a phosphate from ATP to a serine, threonine or tyrosine residue in a protein; phosphatases remove the phosphorylate group. Phosphorylation is the most common post-translational modification on proteins, with approximately 80% occurring on serine, 20% on threonine and 0.1 to 1% on tyrosine residues.

2.4. Inhibition of protein phosphatase

Microcystin and nodularin have been shown to be inhibiting serine/threonine protein phosphatase 1 and 2A. This inhibition leads to hyper- phosphorylation of proteins associated with the cytoskeleton in hepatocytes (Nxusani et al, 2012). Protein phosphatases are group of enzymes, found ubiquitously, which are responsible for the dephosphorylating of various proteins and enzymes in cell. This is an extremely important function in metabolism since protein phosphorylation and dephosphorylating is required for the regulation of a large number of cellular activities. Protein phosphatases were first reported to be inhibited by microcystins (Mackintosh et al, 1990). It was found that extremely low concentrations of microcystin-LR could strongly inhibit protein phosphatases 1 and 2A from both plants and mammals, thereby causing hyper-phosphorylation of the cell and a massive disruption of a number of important cellular mechanisms.

Microcystin-LR consist of the Adda chain amino acid which is the useful tool in microcystin research as it provides the molecules with characteristic wavelength absorbance at 230 nm. This is believed to be attributable to the conjugated diene group in the binding of the toxin to protein phosphatases. The stereochemistry about the diene of the Adda group has been shown

to influence toxicities of microcystins which can differ greatly. The absorbance characteristics of Adda provided a means of analysis of microcystins after separating them by reverse phase HPLC (Michael Dukelow et al, 1990). These enzymes are highly homologous approximately 50% identical and there has been much interest in understanding how such diverse structures might interact with the enzymes. The only structural information for serine/threonine protein phosphatases is derived from a very recent X-ray crystal structure of a cat-PP1 microcystin complex **(**A. P. Mehrotra and D. Gani, 1996).

The phosphatases and proteases may be inhibited by a wide range of compounds with the working concentration range for inhibition in the lower millimolar range (Table 2).

AEBSF. HCl (4-(2-Aminoethyl) benzenesulfonyl fluoride hydrochloride) is a water soluble, irreversible serine protease inhibitor with a molecular weight of 239.5 Da. It inhibits proteases like chymotrypsin, kallikrein, plasmin, thrombin, and trypsin. The specificity is similar to the inhibitor **PMSF** (Phenyl methyl sulfonyl fluoride); nevertheless AEBSF is more stable at low pH values. Typical usage is 0.1-1.0 mM. **EDTA** (ethylenediaminetetraacetic acid) is an amino acid compound, a powerful chelating agent - meaning it attaches to plaque build-up and heavy metals and removes them naturally from the body. EDTA is recognized by the body and easily assimilated.**E-64** is an irreversible, potent and highly selective cysteine protease inhibitor. E-64 is a very useful cysteine protease inhibitor for use in in vivo studies because it has a specific inhibition, it is permeable in cells and tissues, it has low toxicity, it is easily synthesized and it is stable.

Table2: Commonly used phosphatases and proteases and their inhibitors

Inhibitor	Target class	types	Typical working conc.
Sodium fluoride	Serine/threonine and acid phosphatases	irreversible	1 to 20mM
Sodium orthovanadate activation	Tyrosine and alkaline phosphatases	irreversible	1 to 100mM
Beta-Glycerophosphate	Serine/threonine phosphatases	reversible	1 to 100mM
Sodium Pyrophosphate	Serine/threonine phosphatase	irreversible	1 to 100mM
AEBSF.HCl	Serine proteases	irreversible	0.2 to 1.0mM
Aprotinin	Serine proteases	reversible	100 to 200mM
Bestatin	Cysteine protease	reversible	1 to 10uM
E-64	Amino-peptidases	irreversible	1 to 20uM
EDTA	Metalloproteases	reversible	2 to 10mM
Leupeptin	Serine and cysteine proteases	reversible	10 to 100uM
Pepstatin a	Aspartic acid proteases	reversible	1 to 20uM
PMSF	Serine proteases	reversible	0.1 to 10mM

2.4.1 Classification of protein phosphatase

Protein phosphatases fall into two major groups: tyrosine phosphatases and serine/threonine phosphatases based on the amino acid residues from which the phosphate groups are

removed. Serine/threonine phosphatases are further divided into several classes of which PP1, PP2A, PP2B and PP2C (where PP stands for protein phosphatase) are the most known and studied. Serine/threonine phosphatases are classified based on different characteristics (Mackintosh, and Cohen, 1989). Based on substrate favourite, serine/threonine phosphatases are divided into two groups. One group contains PP1 and prefers the β-subunit of phosphorylates kinase as substrate. The other group contains PP2, including PP2A, PP2B and PP2C, prefers the α-subunit of phosphorylates kinase as substrate. Based on ion requirements, Ca^{2+} and Mg^{2+} are required for PP2B and PP2C activity, respectively, while PP1 and PP2A do not have an ion requirement. Based on evolutionary relationships from nucleotide or amino acid sequence comparisons, serine /threonine phosphatases are divided into the PPP (Phosphoprotein phosphatase) and PPM (protein phosphatase member) family

2.4.2 Serine/threonine protein phosphatase 2a

PP2A consisting of 36-kDA catalytic subunit, and is active as either a heterotrimer consisting of one catalytic C subunit and two regulatory A and B subunits or as a heterodimer including only the C and A subunits (Janssen et al, 2001.). The C subunit acts as the catalytic subunit which removes phosphate groups from serine or threonine residues on the substrate protein. In mammals, two different isoforms exist, α and β, which share 86 % sequence identity and are universally expressed. The regulatory subunit B, with several isoforms known, can associate to the core enzyme and regulates the enzyme localization and specific activity of the different holoenzymes (Chamberlin A. Richard et al, 1997). Both isoforms are universally expressed, but PP2ACα is 10 times more abundant than PP2ACβ. This could be explained by the fact that these isoforms are encoded by different genes, and the promoter for PP2ACα is 7–10 times stronger than the promoter for PP2Acβ (Hirota Fujiki1 et al, 2011).

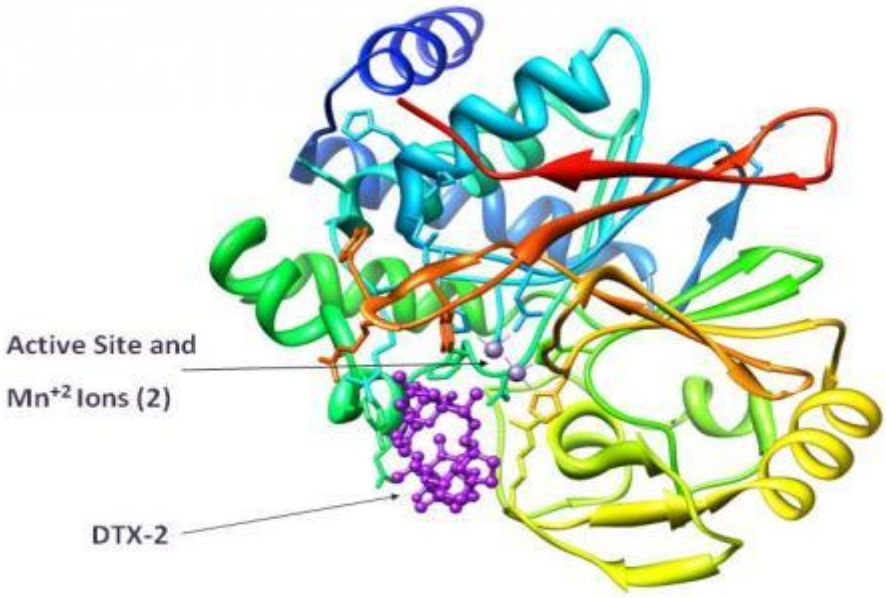

Figure 8 Illustration of PP2A scaffolding and catalytic subunits, with Dinophysitoxin-1 bound to the active site of the catalytic subunit2.5 Toxicity of cyanobacterial to human

Bio-toxins are considered as super-toxin. Bio-toxins of cyanobacteria are water soluble and heat stable and they are released upon aging of the cells. Based on the exposure through dermal contract, animal and human's microcystin or nodularin are concentrated in liver where they are transported to hepatocytes through an active bile acid transport system. These hepatotoxins are known to be resistant to digestion in the gastrointestinal tract of eukaryotes because the peptide bonds linking to the D-amino acids are not susceptible to normal hydrolytic enzymes. They are highly stable in water and are resistant to boiling even to irradiation; thereby presenting a high risk to consumers of animal products which have been contaminated (Msagati et al, 2006). For this reason, the world health organization guidelines for the presence of cyanobacterial cells as shown below table3.

Table.3. Shows summary of WHO guidelines for cyanobacteria levels in drinking water (Msagati et al, 2006)

Risk category	Cell density(cells/ml)	Action recommended
Low risk	20000-100000	None
Moderate risk	>100000	Advisory and possible closure
High risk	Visible scum layer	Closure

Swimming in water that containing toxic blooms of cyanobacteria may expose swimmers to cyanotoxins. Exposure through dermal contact may cause eye, ear and skin irritation, a condition known as dermatitis or swimmers itch or seaweed dermatitis, and gastrointestinal symptoms such as vomiting and diarrhea in bathers (Falconer et al, 2005). MC-LR concentration in waters for human consumption is regulated by environmental Protection Agency (EPA), to a limit of 1 μgL^{-1} MC-LR in drinking waters (WHO, 1999). Current standard methods to monitor MC-LR require sophisticated and expensive procedures and specific laboratorial conditions that take long time to reach the intended result. Within that time the contamination can move/spread out, while users of recreational waters and possible consumers are at risk of contracting serious infections.

2.5. Graphene

Graphene is a one atom layer thick carbon sheet (Hui Zhang et al, 2010). Graphene provides essentially endless possibilities for the modification or functionalization of its carbon backbone (Yong chao Si.et al, 2008). Nanomaterials are becoming popular and useful due to their fascinating and useful characteristics and consequently great application potential. Nanomaterial such as graphene exhibit many interesting electronic, optical and mechanical properties due to its two-dimensional (2D) crystal structure (Rodney S. Ruoff et al, 2010). Graphene has a large theoretical specific surface area 2630 $m^2 g^{-1}$, high intrinsic mobility 200 000 $cm^2 v^{-1} s^{-1}$, high Young's modulus (~ 1.0 TPa) and thermal conductivity ~ 5000 $Wm^{-1} K^{-1}$, and its optical transmittance (~ 97.7%) and good electrical conductivity merit attention for applications such as transparent conductive electrodes, among many other potential applications (Chen et al, 2011).

Graphene is a building block of carbon material because it can be wrapped up to form fullerenes of all types of dimensions, rolled-up to form carbon nanotube or stacked up to form graphite. All of the variation from graphene exhibit interesting electrical properties, which have been explored in literature. Graphene has been experimentally studied for over 40 years, and measurements of transport properties in micromechanically exfoliated layers, of graphene grown on (SiC), large area graphene grown on copper (Cu) substrates, as well as a variety of studies involving the use of chemically modified graphene (CMG) to make new materials, have in part led to a flow in the number of publications and in the amount of, e.g., National Science Foundation grants recently awarded in the USA alone (Ruoff et al, 2010)

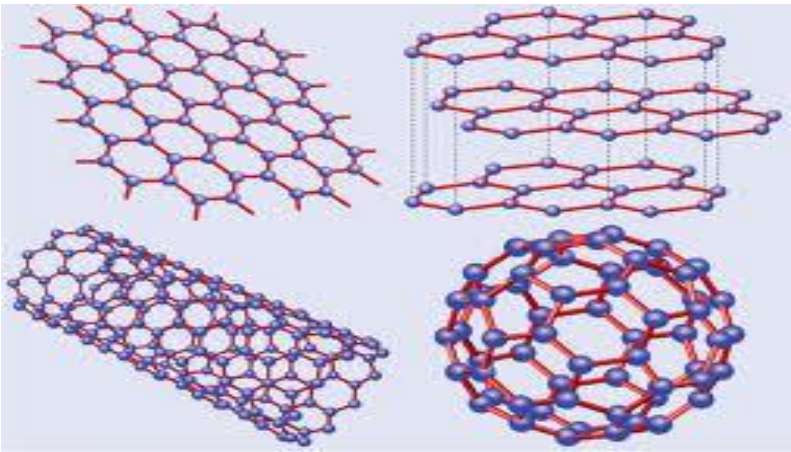

Figure 9 Graphene and its descendant structures

2.6 Graphene oxide

Graphene oxide contains a range of reactive oxygen functional groups, which renders it a good candidate for polymer composites, sensors, energy related material, field effect transitions and for biomedical uses. Its application may be extended through harnessing mechanical, electrical and thermal properties using chemical functionalization (Rodney S. Ruoff et al, 2010).

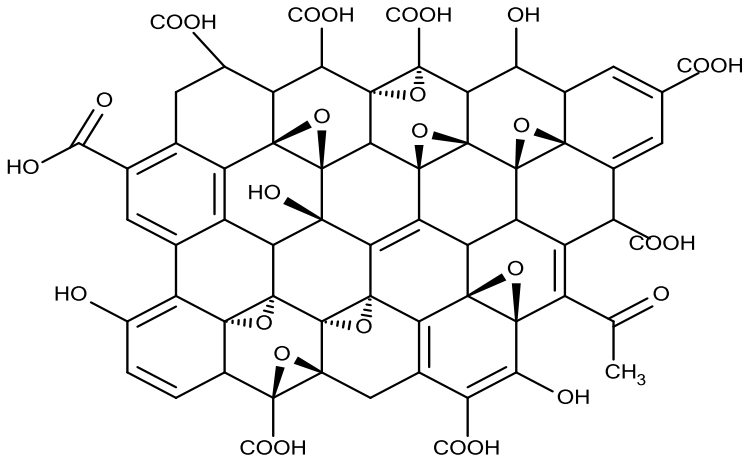

Figure 10 Structure of graphene oxide

2.7. Polyamic acid

Polyamic acid is a precursor of polyimides which are well-known as important extraordinary performance polymers. Polyimides are a group of thermally stable polymers that are often founded on inflexible aromatic backbones. Polyimides are produced by the condensation reaction of an aromatic dianhydride and aromatic diamine to form an oligomer of amic acid known as polyamic acid which act as a precursor for polyimide and can be further cyclized (imidization) by thermal means to produce polyimide. Out of the many types of aromatic polyimides produced worldwide, the largest market and most preferred polyimide for various applications is based on the Pyromellitic dianhydride (PMDA) and 4,4′-oxydianiline (ODA) (Singh et al, 2008). From literature, it is evident that PAA is a promising polymer matrix for various sensor applications. The carboxyl and amine functionalities have been employed in the design and fabrication of derivatives polymer platforms for applications (Noah N et al, 2012).

Numerous researches on the syntheses and applications of aromatic polyimides have been reported over the past few decades due to their dielectric properties with high thermal stability while few researches that has been conducted to polyamic acid (Kakimoto et al, 2000). As a result polyimide has been used in applications ranging from adhesives, thermal resistant coatings, high performance composites, fibres, foams, membranes, mouldings and films. Poly (amic acid) (PAA) films could open up the possibility of creating poly-functional materials because of the presence of amide and carbonyl functionalities. On average functionality in PAA can vary from 160 to 600 depending upon its molecular weight (Sadik, 2010). PAA showed good solubility in strong acid as well as in aprotic solvents, such as Dimethylacetamide, NMP, and DMSO, but heat-treated samples at higher temperatures showed poor solubility in the same solvents (Wang et al, 2010).

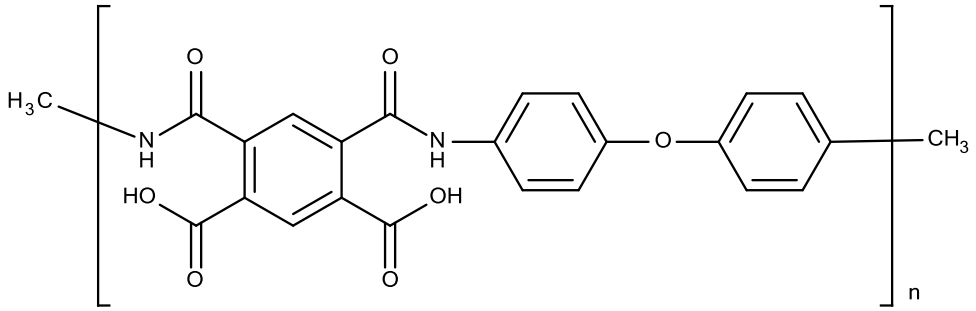

Figure 11: Structure of polyamic acid

CHAPTER 3

This chapter describes the various techniques employed, provides the study methodology and experimental procedures for the electrochemical synthesis of graphene oxide with polyamic acid conducting polymer composites. Details regarding biosensor construction, as well as enzyme linked immunosorbent-assay protocol will also be provided.

Material and methodology

3.1. Reagents and materials

The following chemicals were obtained from Sigma Aldrich: 4, 4′-oxydianaline (ODA), Pyromellitic dianhydride (PMDA), N, N-Dimethylacetamide (DMAc), concentrated H_2O_4 (98%), graphite powder, $KMnO_4$, H_2O_2 (30%), HCl (10%), Microcystins-ADDA ELISA ABRAXIS KIT (microtiter plate). The enzyme serine/threonine protein phosphatase 2a was purchased from biocom-biochem. 0.1 M, pH 7.3 saline was prepared from anhydrous disodium hydrogen phosphate (Na_2HPO_4), sodium dehydrogenase phosphate (NaH_2PO_4) and sodium chloride (NaCl). Deionized water purified by a milli-QTM system (Millipore) was used for all aqueous solution preparations.

3.2 Methodology

3.2.1 Synthesis of polyamic acid

Polyamic acid was synthesised by stirring a mixture of 2.0024 g (0.01 moles) of N, N-Dimethylacetamide (ODA) in 157 mL of acetonitrile (ACN) until solvation. Then, 50 mL of acetonitrile (ACN) containing 2.1812 g of Pyromellitic dianhydride (PMDA) (0.01 moles) was added dropwise over 1 h and the solution was stirred for 24 h. The resulting precipitate was filtered under suction and dried at room temperature. A yellow powder was obtained at a yield 3.351 g, following the synthesis previously proposed (Sadik, 2000).

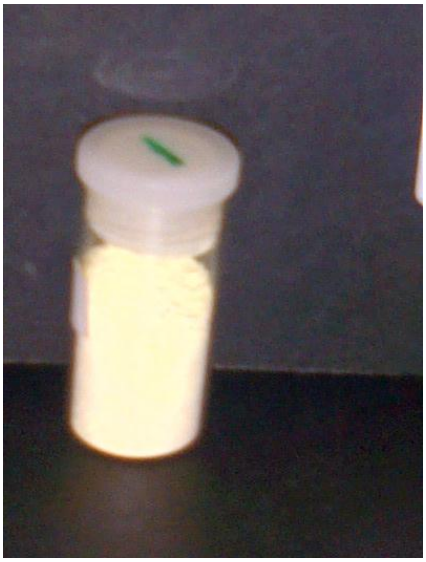

Figure 12: Polyamic acid in powder form

3.2.2 Synthesis of Graphene oxide

Graphene oxide was synthesised using Hummers method starting with 2g of graphite powder, added to 1 g of sodium nitrite ($NaNO_3$) and 50ml of sulphuric acid (H_2SO_4) in a conical flask. After stirring 30 min at room temperature the solution was placed in an ice bath and was allowed to stir for a further 20 min. 7g of potassium permanganate ($KMnO_4$) was added gradually to the solution with continued stirring in the ice bath. The solution was removed from ice bath and was allowed to stir at room temperature for 20 min after which the conical flask was placed in water bath at 35º C and was left to stir for 3hours. The conical flask was returned to the ice bath with stirring while 150ml of water was slowly added to the solution. Afterwards 5ml of hydrogen peroxide was slowly added until bubbles disappeared. The conical flask was removed from ice bath and allowed to stir at room temperature overnight. The solution was placed into smaller tubes and centrifuged for 20 min after which the liquid layer was removed. 1: 9 mixtures of HCL and distilled water (H_2O) were added to the tubes and then it was centrifuged for 20 minutes. These centrifugation steps were repeated at least

three times and the remaining solution was covered with tissue paper and parafilm. It was then placed in vacuum oven to dry for 3 days after which a brown product was obtained.

Figure 13: Graphene oxide synthesis product

3.2.3 Characterization of PAA, GO and composite of PAA: GO using GCE

3.2.3.1 Preparation of Graphene oxide (GO)

Glassy carbon electrode were cleaned with 0.1, 0.3 and 0.05µm aluminium slurries followed by sonication with ethanol and washing with distilled water to ensure that the working electrode was clean. The counter electrode used was a platinum wire and the reference electrode was Ag/AgCl (3M NaCl). The electrochemistry experiments were carried using BAS 100W electrochemical workstation. Synthesised GO was dissolved in distilled water (1mg/ml) and electrochemically deposited onto GCE by cycling between -1300 to 550 mV (vs. Ag/AgCl) until stable thin layers of GO gradually deposited onto the surface of the glassy carbon electrode.

3.2.3.2 Preparation of Polyamic acid (PAA)

The glassy carbon electrode was sonicated in ethanol and then rinsed with distilled water to clean the working electrode. PAA was dissolved in DMAc to produce a 50mg/ml solution

which was degassed with Argon to remove dissolved oxygen. PAA was then electrochemically deposited onto glassy carbon electrode by cycling between 550 mV to -1300 mV (vs. Ag/AgCl) at a scan rate of 100 mV s^{-1}, for 50 cycles. PAA thin films produced was characterised in 0.1M PSB (pH= 7.3) at scan rates from 10–100 mVs^{-1} to evaluate the redox behaviour of polyamic acid. Higher scan rates were not used, since it is known that PAA exhibits diffusion controlled electrochemistry at low scan rates.

3.2.3.3. Preparation of Polyamic acid (PAA)–Graphene oxide (GO) composites

Using a similar three electrode cell, potential window and scan rate PAA-GO thin films were co-deposited from a solution containing $2.5x10^{-6}$ mole PAA and $1.27x10^{-5}$ mole GO dissolved in 0.1M PSB to produce the 20:80 composite thin film in situ. The resulting PAA: GO modified glassy carbon electrode was characterised at different scan rate (10 to $100mVs^{-1}$) as before PAA: GO composite films from 50:50 and 80:20 starting ratio was also prepared in the same way.

3.2.4 Preparation of serine/threonine protein phosphatase 2a stock solution

The stock solution of the serine/threonine PP2a was purchased with phosphate buffer solution of 1ml, which we then mixed with 1ml of phosphate buffer and stored in the fridge at -4 ºC.

3.2.5 Preparation of biosensor

The electro-deposition of PAA:GO composite onto cleaned glassy carbon electrode was followed by containing 5.0 x 10^{-6} mole of polyamic acid, 2.53 x10^{-5} mole of graphene oxide and 2ml 0.1M PSB pH7.3. After electro-polymerisation and deposition of PAA: GO onto GCE, the modified electrode was then placed into 1nM PP2a solution to incubate for 120 seconds. In this way the GCE/PAA: GO/PP2a biosensor was produced, which was further characterised in phosphate buffer. After characterization, the biosensor GCE/PAA: GO/PP2a was used for quantitative determination of microcystin-LR concentration.

3.2.6 Preparation of microcystin-LR standards solution

0.1µg/ml working solution (0.0197ml) of Microcystin-LR was prepared from 10.128µg/ml of stock solution (microcystin-LR, 1ml). Working solution (microcystin-LR) was diluted to produce standards at 0.5, 1.0, 1.5, 2.0, 2.5nM concentration each of 3ml total volume in distilled water.

3.2.7 Preparation for scanning electron microscopy (SEM)

Thin films of the PAA: GO composites were prepared by electro-polymerisation onto screen printed carbon electrodes. After electrodeposition, the PAA: GO modified electrodes were left to dry in air before SEM analysis. The SEM analysis was performed on a Hitachi Model X-650 Scanning Electron Micro analyser from Tokyo, Japan coupled to Energy Dispersive X-ray Analyser. Samples were mounted on aluminium stubs using conductive glue and coated for viewing with a thin layer of gold.

3.2.8 Preparation of enzyme linked immunosorbent assay (ELISA)

First step: 90 wells microplates was used for analysis by ELISA. 50µL of all standard solutions and control from the Abraxis kit was added into the wells of the test strips. In same step 50µL of waste tap water and distilled water (real samples) was added into test strips. 50µL Antibody solution from the kit was added to the individual wells successively before covering and mixing by shaking for 30 seconds. After the test strips were incubated for 90 minutes at room temperature, the parafilm was removed and the strips were washed using 1X wash buffer solution, three times. The remaining buffer in the wells was removed by patting the plate dry on a stack of paper towels.

Second step: 100µL of Enzyme conjugate solution was added to the individual wells successively. The wells were covered and after mixing for 30seconds, the strips were incubated for 30minutes at room temperature. The strips were washed as before and dried on paper towels.

Third step: 100µL of substrate (colour) solution was added to the individual wells and allowed to incubate for 30 min at room temperature. Afterwards, 50µL of stop solution was added to the wells. Analysis of microplate using ELISA photometer (450 nm) was done within 15 minutes after the addition of the stopping solution.

3.2.9 Preparation of samples for Atomic force microscopy (AFM)

Electro-polymerisation of the PAA, GO and PAA: GO composites was done onto GCE as detailed before, after electro-deposition, the PAA: GO modified electrodes were left to dry under UV lamp, before AFM analysis. The AFM analysis was performed on Nanosurf easy Scan 2, this technique is a system that can make nanometre scale resolution measurements of topography and several other properties of a samples. In this study was used to study morphology of all PAA: GO composites and individual of PAA and GO synthesized in situ.

3.2.10 electrochemical impedance spectroscopy (EIS)

A three electrode system, same as that used for electrodeposition of the composites was used in this characterization. The characterization solution contained 2mL of 0.1 M PBS. The response of the biosensor to microcystin was evaluated in the concentration range 0.5 to 2.5 nM.

3.3 Measurement and instrumentation

Cyclic voltammetry and Square wave experiments were carried out using a BAS100W integrated and computerized electrochemical work station from Bio Analytical Systems (BAS), Lafayette, USA or the Volta Lab PGZ402 (Radiometer Analytical SAS, Lyon, France) electrochemical workstations. Throughout a three electrode electrochemical cell was used with glassy carbon working electrode (A = 0.071 cm^2) from BAS, platinum wire as counter electrode (Sigma Aldrich) and Ag/AgCl (3M NaCl) reference electrode.

Ultra violet-visible spectroscopy measurements were made on a Nicolet Evolution 100 UV-visible spectrometer (Thermo Electron, UK), using a quartz cuvette. Attenuated Total Reflectance Fourier Transform Infrared spectra (ATR-FTIR) were recorded in the range of 4000-300 cm^{-1}using a PerkinElmer Model spectrum 100 series for graphene, graphene oxide, polyamic acid and the composites of graphene oxide-polyamic acid.

Electrochemical impedance spectroscopy (EIS) measurements were recorded with Zahner Elektrik IM6 electrochemical work station at a bias potential of 0V, amplitude of 5mV; recorded at a frequency range of 100 MHz to 100 KHz. Electrochemical cell with a three electrode set up was used.

PH meter was also used to measure the pH of all phosphate buffer solution for biosensor application. Screen printed carbon electrodes (Dropsies, Spain) were used as working electrodes to prepare samples for SEM and AFM analysis. Alumina micro polish and polishing pads were obtained from Buehler, IL, USA and were used for polishing the glassy carbon electrode before all experiments.

3.3.1 Voltammetry

Voltammetry has its roots from the discovery of polarography in 1922 by the Czech chemist, Jaroslay Heyrovsky, for which he was subsequently honoured by the 1959 Nobel Prize in chemistry. In this regard, voltammetry is based on exactly the same principles that pertain to polarography. In a more definitive context, generally, the common feature shared by all voltammetry techniques is the application of potential (E) to the working electrode and the monitoring of the resulting current (I) flowing through the electrochemical cell. Depending on the particular type of voltammetry technique, the potential may either be scanned between selected potentials (E1 and E2), or the potential of the working electrode may be changed instantaneously, whereas the resulting current may be monitored as a function of potential or time depending on the type of voltammetry technique.

3.3.2 Cyclic voltammetry method

It is a technique which is widely used in the study of oxidation/reduction reactions and the detection of reaction intermediates. It offers a rapid location of redox potentials of the electro-active species (Andrienko, 2008). The purpose of cyclic voltammetry is to offer qualitative information about electrochemical processes under various conditions. In a cyclic voltammetry experiment the working electrode potential is ramped linearly versus time as in linear sweep voltammetry, but at the end potential the direction is reversed to provide oxidation and reduction in one single (or multiple) sweep (figure 14).

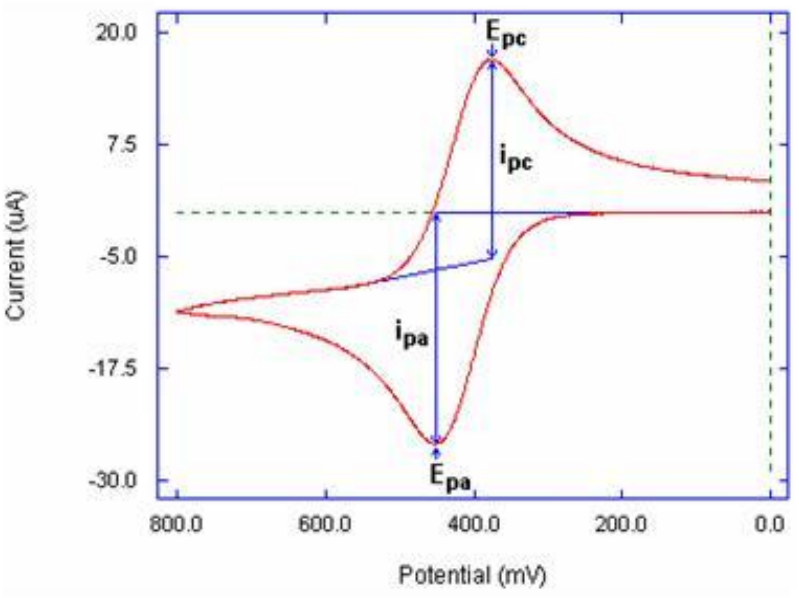

Figure 14: Cyclic voltammogram of a reversible reaction, indicating peak currents for oxidation and reduction

Cyclic voltammetry can distinguish between reversible, quasi- reversible or irreversible systems.

(i) **Reversible process**: occurs when an electro-active species in solution is oxidized (reduced) in a forward scan and reduced (oxidized) in the backward scan. This type of system is in equilibrium throughout the potential scan and if the electro-active reactant (Ox) is dissolved in an electrolyte solution of sufficient conductivity and the electrochemical reaction is not extensive enough to alter the composition of the bulk of the electrolyte, the product (Red) is stable and also soluble in the electrolyte, the following reversible electrode reaction:

$$\Delta Ep = Epa - Epc = 2.3\frac{RT}{nF} \approx \frac{0.058}{n}v \quad \text{at } 25^{o}C \text{ and,} \qquad \text{(Equation 1)}$$

When the reduction process is reversible, the peak current is again given:

$$I_{pc} = 0.4463nFA\,[\frac{nF}{RT}]^{1/2}\,C^{b}_{ox}\,D^{1/2}_{ox}\,V^{1/2} \qquad \text{(Equation 2)}$$

$$I_{pa} = 0.4463nFA\,[\frac{nF}{RT}]^{1/2}\,C^{b}_{red}\,D^{1/2}_{red}\,V^{1/2} \qquad \text{(Equation 3)}$$

In term of adjustable parameters, the peak current was given by the Randles-Sevcik equation. This equation describes the effect of scan rate on the peak current $\mathbf{I_p}$. The equation was given by-

$$I_p = 2.69 \times 10^5 n^{3/2} A D^{1/2} C^b v^{1/2} \quad \text{at } 25^oC \qquad \text{(equation 4)}$$

Where **ip** = Peak Current in A, **n** = 1 number of electrons, **F** = 96485 C mol^{-1} Faradays Constant, **A** = 0.071 cm^2 geometric area of the electrode, **R** = 8.314 J mol^{-1} K^{-1} Gas Constant, **T** = 298.15K absolute Temperature and **ν** = Scan Rate in V s^{-1}.

(ii) Irreversible process :is the process where the reaction goes one-way, the most common is when only a single oxidation or reduction peak with a weak or no reverse peak is observed. Irreversible processes are a result of slow electron transfer or chemical reactions at the surface of the working electrode. A large peak potential separation between **Epa** and **Epc** also indicates an irreversible reaction, if there is a return peak.

$$\Delta Ep = Epa - Epc > 2.3\frac{RT}{nF} \approx \frac{0.058}{n}v \quad \text{at } 25^oC \text{ and,} \qquad \text{(Equation 5)}$$

$$I_{p,c} = 0.4958 \text{ x } nF \text{ x } (\frac{\alpha nF}{RT})^{1/2}\,A\,Do^{1/2}\,V^{1/2}\,C^{b}_{o} \qquad \text{(Equation 6)}$$

(iii) Quasi-reversible: process exhibits behaviour which lies between the reversible and irreversible processes, active species in solution is oxidized (or reduced) in a forward scan and reduced (or oxidized) in the backward scan. This type of system is in equilibrium throughout the potential scan. Reversibility requires that the electron transfer kinetics is fast enough to maintain the surface concentrations of

O and R at the values required by the Nernst equation. Hence, reversibility depends on the relative values of the standard heterogeneous electron transfer rate constant (ks) and the rate of change of potential - the scan rate n. If the ratio of ksn^{-1} is sufficiently small that Nernstian concentrations cannot be maintained, then the process is said to be quasi-reversible. A quasi-reversible process is characterized by:

$$DEp > 59.2/n \text{ mV}, \qquad \text{(Equation 7)}$$

with the value increasing with increasing n

3.3.3 Square-wave voltammetry

Square wave is a further improvement of staircase voltammetry which is itself a derivative of linear sweep voltammetry, it is a technique that is similar to cyclic voltammetry, but is much more sensitive than cyclic voltammetry. SWV is more advantageous compared to CV since it includes excellent sensitivity and rejection of back ground current. In square wave voltammetry the entire scan speed can be very high. This high speed coupled with computer control and signal averaging allows for experiments to be performed repetitively and increases the signal to noise ratio. The peak height is directly proportional to the concentration of the electro-active species and direct detection limit as low as 10^{-8} M is possible (figure 15). SWV may also be applied in study of electrode kinetics with regard to preceding, following or catalytic homogeneous chemical reactions and determination of some species at trace levels.

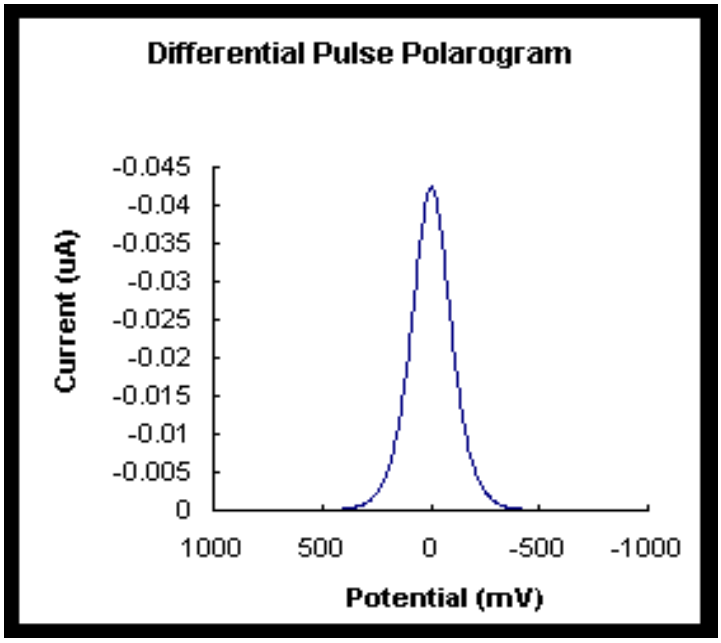

Figure 15: Illustration of square wave voltammetry

A series of Voltammetry techniques such as cyclic voltammetry and square-wave voltammetry have been used in this study, for electrochemical characterisation of different synthesised thin film composites onto glassy carbon electrode surface as well as their response to microcystin LR.

3.3.4 Ultra violet-visible spectroscopy

Uv-vis spectroscopy is used to probe the electronic transitions of molecules that absorb light in the ultraviolet and visible region of the electromagnetic spectrum and is considered a reliable and accurate analytical technique for the qualitative as well as the quantitative analysis of samples. When sample molecules are to light having an energy that matches a possible electronic transition within the molecule, some of the light energy will be absorbed as the electron is promoted to a higher energy orbital. It uses light in the Uv-vis region of the spectrometer or in the ranges near infrared to excite the sample, where upon the sample

absorbs some of the light these electronic transitions can provide the properties of substances such as structure and colour and energy associated with each transition.

Beer-Lambered Law is used for estimation of concentration of light absorbing species as the light passes through it and is given by:

$$A = -\log_{10}\left(\frac{I0}{I}\right) = \mathcal{E}\ .c.L \qquad \text{(Equation 8)}$$

The equation above **A** is the absorbance of light which is directly proportional to the concentration of the absorbance, $\mathbf{I_o}$ is the intensity of incident light, **I** is the intensity of the transmitted light, **Ɛ** is the molar absorptivity and L is the path

3.3.5 Electrochemical impedance spectroscopy (EIS)

Electrochemical impedance spectroscopy is a power diagnostic tool used characterizes electrode processes and complex interfaces. During an impedance measurement, a frequency response analyser (FRA) is used to impose a small amplitude AC signal to an electrochemical cell, The AC voltage and current response of the cell is analysed by the FRA to determine the resistive, capacitive and inductive behaviour of the cell at that particular frequency. EIS data are most often represented in Nyquist and Bode plots. Bode plots refer to representation of the impedance magnitude (or the real or imaginary components of the impedance) and phase angle as a function of frequency. They explicitly show the frequency-dependence of the impedance of the device under test. A complex plane or Nyquist plot depicts the imaginary impedance, which is indicative of the capacitive and inductive character of the cell, versus the real impedance of the cell. Nyquist plots have the advantage that activation-controlled process with distinct time-constants show up as unique impedance arcs and the shape of the curve provides insight into possible mechanism. It can reach high time resolution (10^{-6} s) and

is particularly suitable to the study of reaction mechanisms (effects of the surface energetic), current density distribution (effects of electrode geometry), and transport of mass (diffusion and migration in the bulk). Electrochemical Impedance Spectroscopy can even be used to test the quality of food (J. Food Science, 2000).

The spectroscopic tools such as Ultra violet visible spectroscopy, FTIR, and electrochemical impedance spectroscopy were used to evaluate chemical changes at the glassy carbon electrode interface after each modification step. Surface morphology was analysed by scanning electron microscopy and atomic force microscopy. Cyclic voltammetry, square wave voltammetry and impedance analyses were done to investigate the concentration dependent behaviour of microcystin-LR binding to phosphatase biosensor.

CHAPTER 4

Here we present the results of morphology, spectroscopy and electrochemical evaluation of Graphene oxide (GO), Graphene (G), Polyamic acid (PAA) and the novel compounds synthesized by in situ electrochemical polymerisation.

4.1 Microscopy

4.1.1 Scanning electron microscopy

The scanning electron microscope (SEM) uses a focused beam of high-energy electrons to generate a variety of signals at the surface of solid specimens. SEM analysis performed on graphene oxide (GO) thin films onto screen printed carbon electrodes revealed that the GO was entirely exfoliated as individual GO sheets (figure 16 A) and good quality sheets were formed due of similar appearance to literature reports, using the same method of preparation (Chengbin Liu, 2010: Kotseng et al, 2013). Graphene consists of randomly aggregated thin crumpled sheets closely associated with each other and forming a disordered solid. The folded sheets were found to be ~ 2nm in size (Christopher W. Bielawski and Rodney S. Ruoff, 2009). Graphene (figure 16 B) was compared with graphene oxide and the absence of a web-like graphene network, confirmed the successful chemical conversion.

SEM of (PAA) (figure 16 C) showed an amorphous crystalline surface morphology in the order of 200nm range. EDS picked could quantify the carbon and oxygen as mass percentage, but nitrogen could not be quantified.

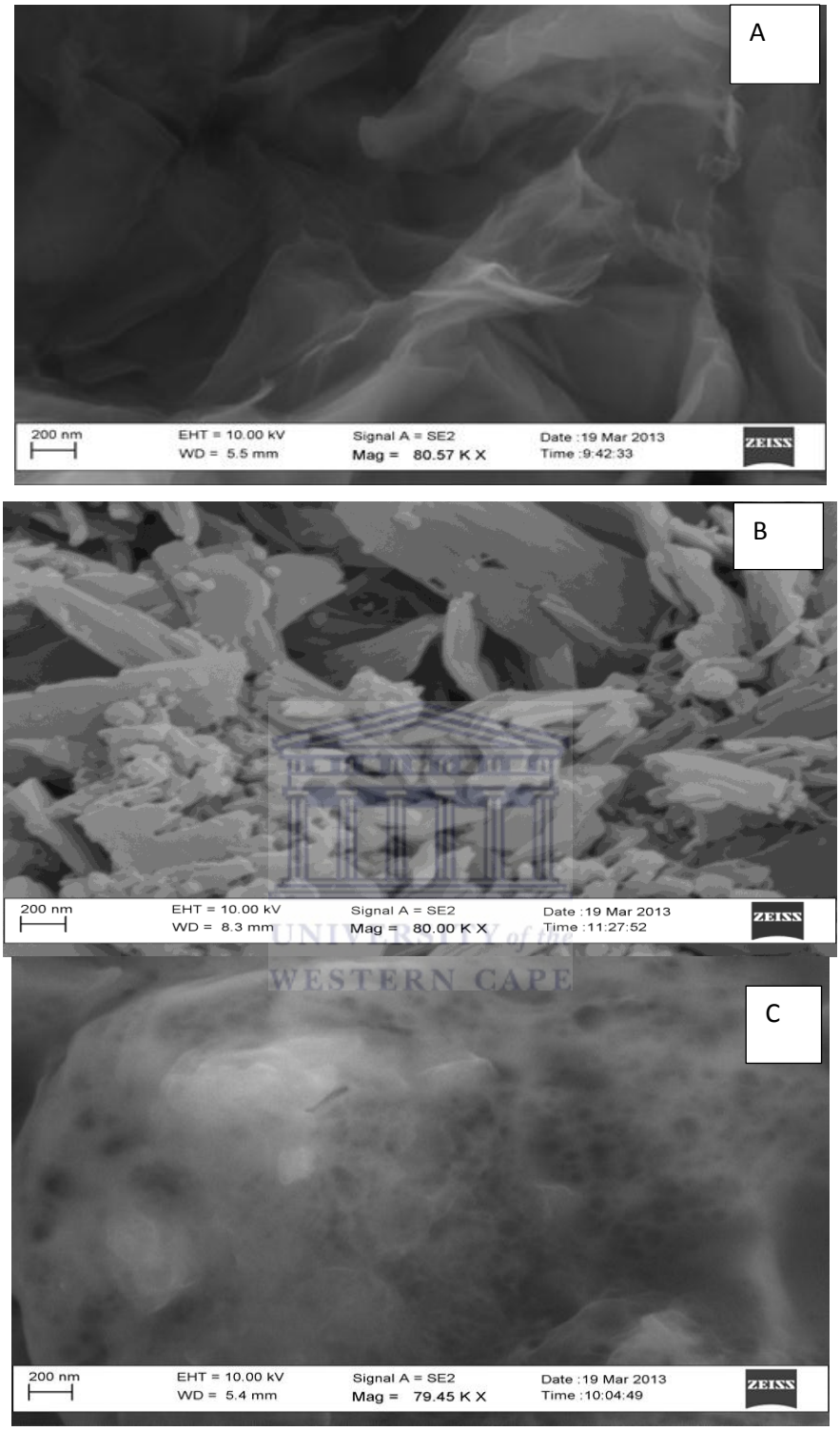

Figure 16: SEM of (A) Graphene oxide, (B) Graphene and (C) Polyamic acid

4.1.2 SEM of newly formed composites

GO and PAA was controlled by molar ratio in the synthesis solution to yield 50:50, 80:20, 20:80 as starting solutions for electrochemical synthesis of composites. At all three ratios it was evident that PAA formed a homogeneous deposit onto GO sheets (figure 17 A, B, C). The 50:50 synthesis mixtures produced a homogeneous composite of GO: PAA where neither one component dominated the morphology.

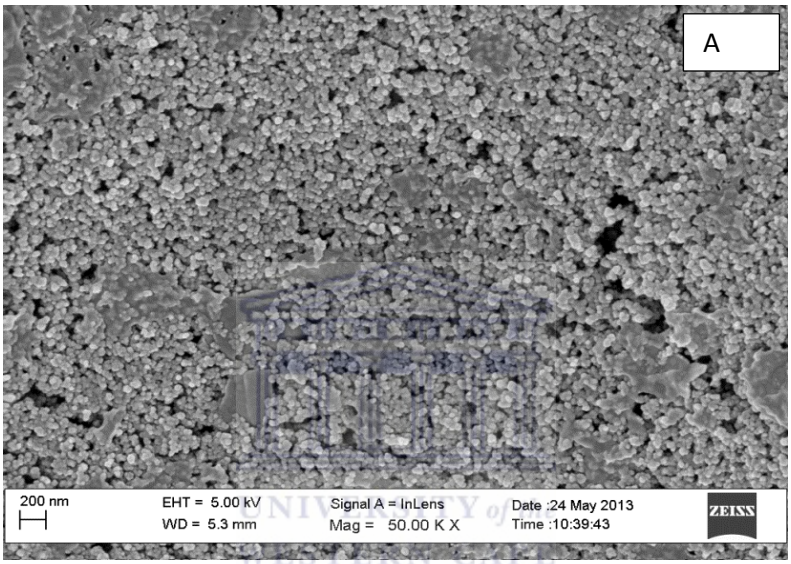

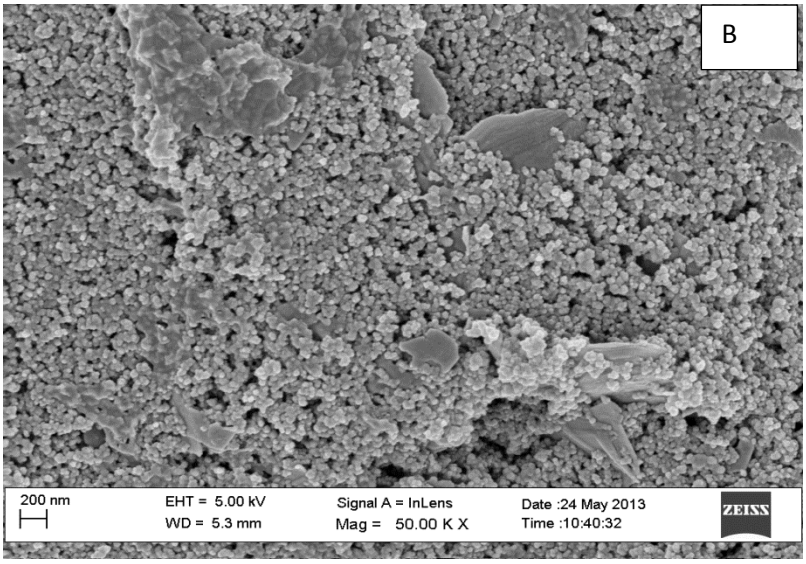

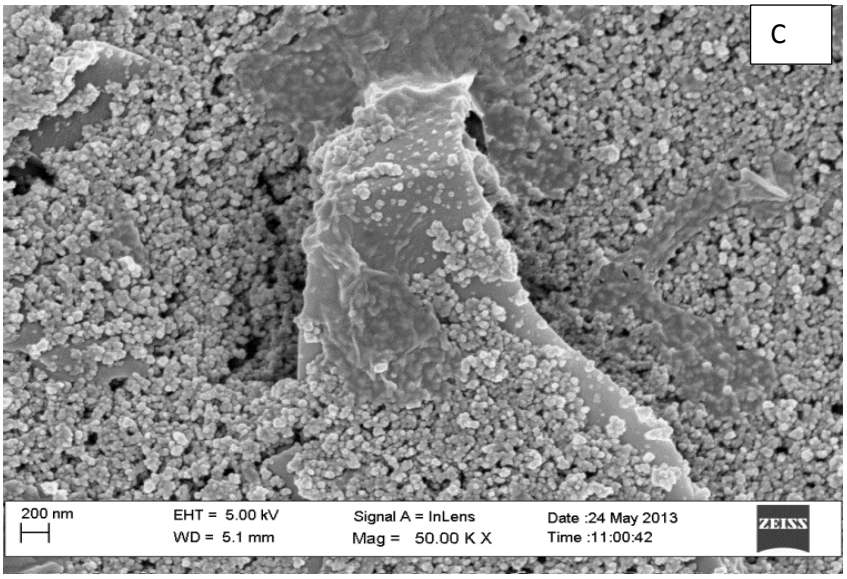

Figure 17: SEM of screen printed carbon electrode modified with (A) PAA: GO (50:50), (B) PAA: GO (80:20) and (C) PAA: GO (20:80).

In the composite where GO was the dominant starting material clear evidence of graphene oxide sheets were visible, with PAA growing onto the template offered by the sheets and with each sheet separated by PAA polymer deposit (figure 17 C).

4.1.3 Atomic force microscopy

Atomic force microscopy is a technique that provides 3D imaging of a material's surface. A standard cantilever with tip sitting on a flexible arm was used to apply small forces. The probe was used to feel the surface like a mechanical arm in AFM tapping mode, to obtain topography imaging of polymers and new composites.

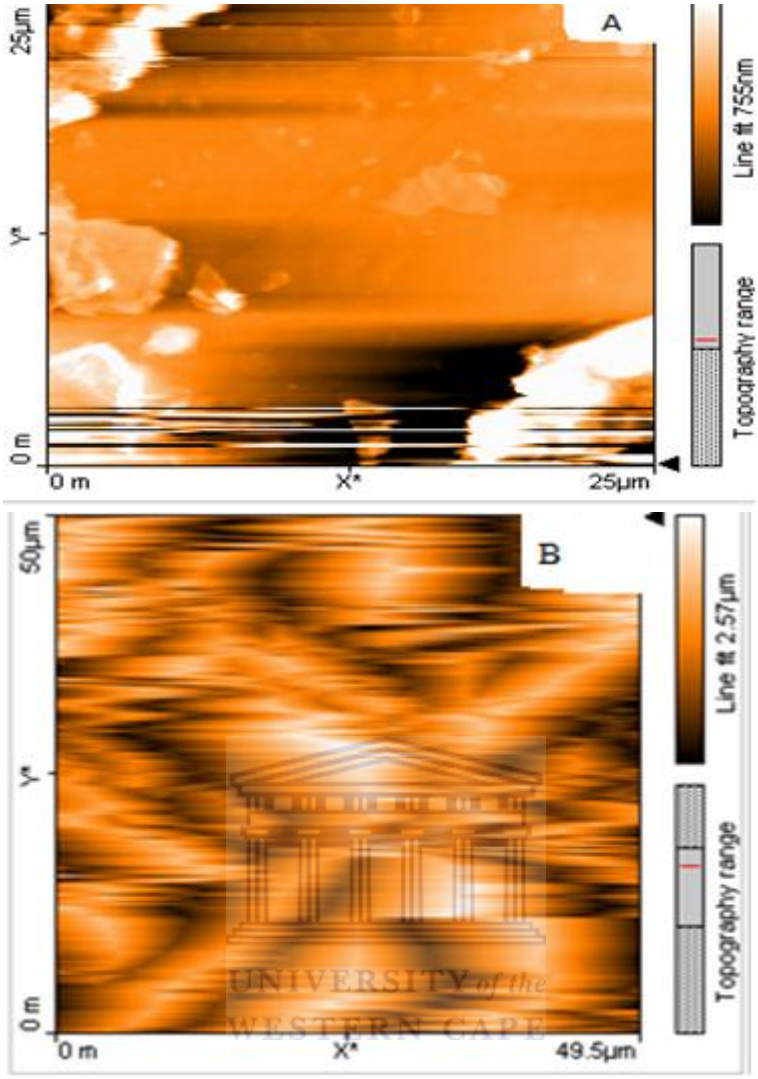

Figure 18: Topography imaging by AFM of (A) Graphene oxide and (B) polyamic acid deposited onto GCE

AFM shows uniform layers of GO Sheets adsorbed onto glassy carbon electrode with roughness = 65.373 nm. The graphene oxide was expected to be dense due to the presence of covalently bonded oxygen and the displacement of sp^3 hybridised carbon atoms, slightly above the original graphene plane, providing a smooth sheet like topography (Li. Zhuang; Lee. Sungho et al, 2012). The polyamic acid.electrochemically deposited onto GCE, showed a clearly Zig -Zag patterned morphology with roughness = 354.42 nm.

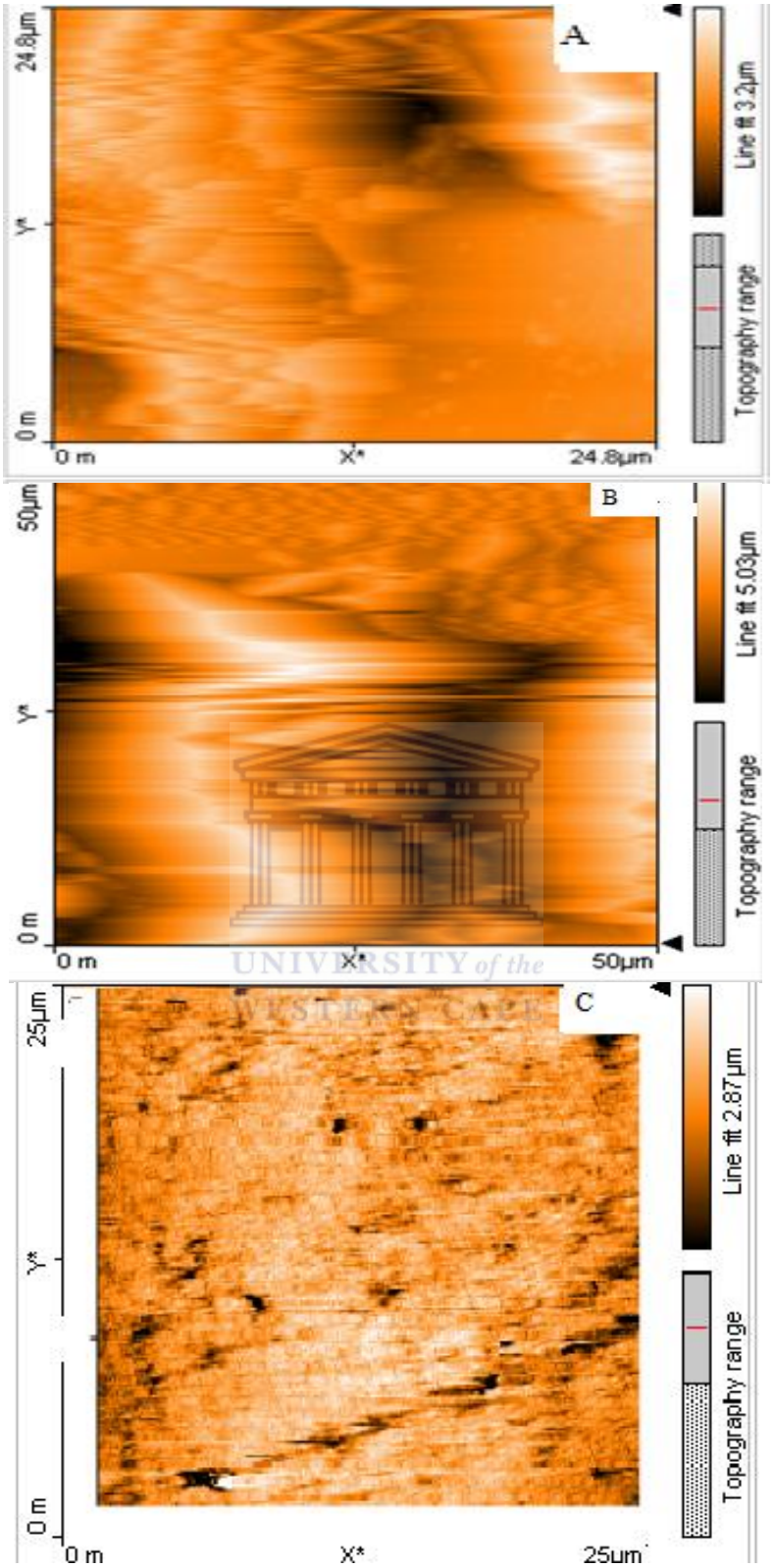

Figure 19: Topography imaging by AFM of (A) 20:80, (B) 80:20 and (C) 50:50 GO: PAA nanocomposites electro synthesised.

When PAA or GO was present as the dominant ratio, the resulting composite reflected its morphology. The 50:50 composite showed a morphology and roughness distribution consistent with uniform incorporation of both PAA and GO. These observations support the morphology also observed by scanning electron microscopy.

4.2 Spectroscopy

4.2.1 Fourier Transform Infrared spectroscopy (FTIR)

FTIR was obtained using Bruker-Tensor 27 spectrometer. The FTIR analyses of composite GO: PAA and unmodified polyamic acid, graphene oxide and graphene were recorded over the range of 450cm^{-1} to 4000cm^{-1}. Polyamic acid, graphene oxide and graphene were recorded as powder. Mixtures of PAA and GO were prepared by volume to represent the ratio control envisaged for nanocomposites. PAA dissolved in DMAc and graphene dissolved in distilled water produced homogeneous mixtures within their respective ratios by volume, which were analysed in a solution cell for evidence of cross linking. Graphene analysis was recorded for comparison of functional groups to graphene oxide, to confirm that GO was indeed formed.

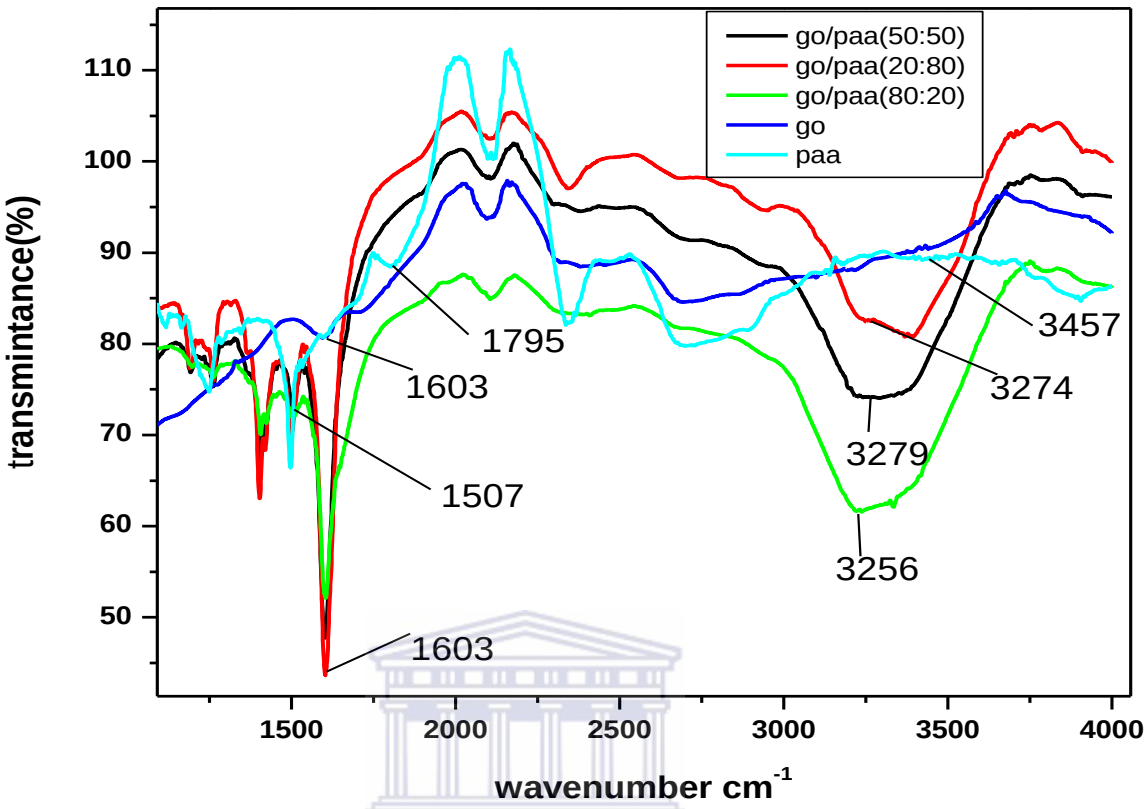

Figure 20: FTIR spectra of PAA: GO nanocomposites, graphene, graphene oxide and polyamic acid

The absorption bands that occur at around 2684cm^{-1} (broad) and 1825 cm^{-1} assign to vibrational mode of carboxylic acid whereas the bands occurring at 3278cm^{-1}, 3317 cm^{-1} and 3301cm^{-1} can be assigned to vibrational mode of (N-H) stretch of PAA. The spectrum of graphene oxide on its own gave a (C = C) stretch at around 15 84cm^{-1}and a peak at 1850cm^{-1} due to carbonyl. This confirmed the presence of carboxylic and hydroxyl group in GO. GO: PAA composites reflected these same vibrations with intensities representative of ratio control during synthesis. A proposed structure for the crosslinking of PAA and GO to

produce the nanocomposites is provided (figure 21) indicating the possibility of ester formation between carboxylic acid groups on PAA and OH of graphene oxide.

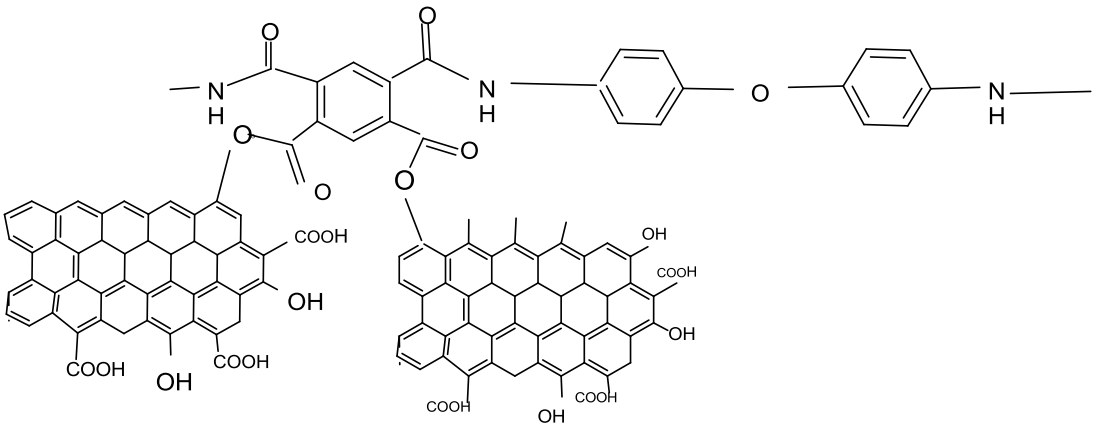

Figure 21: Proposed cross-linked structure of PAA: GO nanocomposites

.

4.2.2 Uv-vis absorption spectroscopy

The absorption spectrum of graphene oxide was recorded from wavelength of 200nm to1100nm. The spectrum of graphene oxide has absorption peak at 230nm which is shifted to 270nm in graphene (figure 22). This is called a red shift which is due to electronic configuration in graphene in the reduction of graphene oxide. From this the band gap energy of the graphene oxide was found to be 5.37 eV equivalents to 8.61 $x10^{-19}$ J, calculated using the following formula:

$$E = \frac{hc}{\lambda} \qquad \text{. (Equation 9)}$$

Where E is the band gap energy, h = 6.626 x 10^{-34} J.s is Planck's constant, c = 2.99 x 10^{8} ms^{-1} is the speed of light, λ in (nm) is the experimental optical absorption wavelength. GO is proportional to the concentration of the oxygen atoms, and this band gap reveal that graphene oxide is a non-metal. In the spectrum of GO, there was a typical absorption at 230 nm and a shoulder around 300 nm, which arose from π-π* transitions of C-C aromatic rings and n-p*

transitions of C-O bonds respectively. The band gap of graphene on the other hand is closer to what is typically expected for metals and/ or semiconductors.

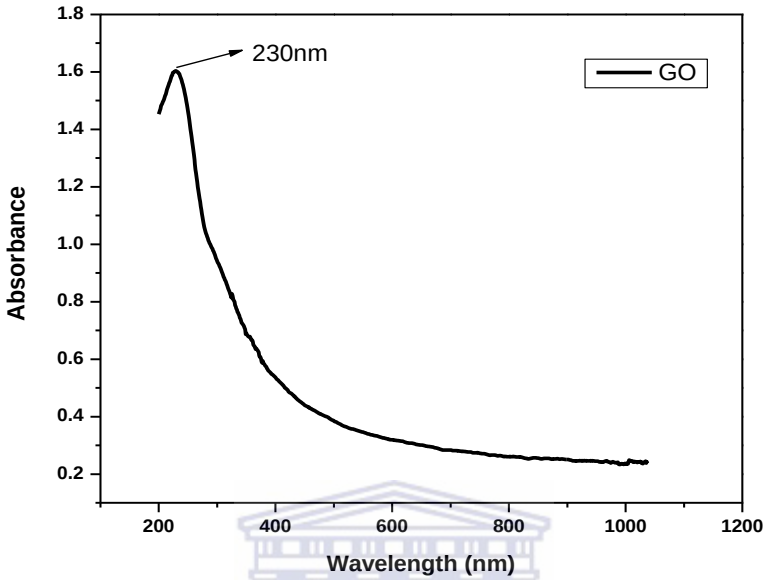

Figure 22: Proposed cross-linked structure of PAA: GO nanocomposites

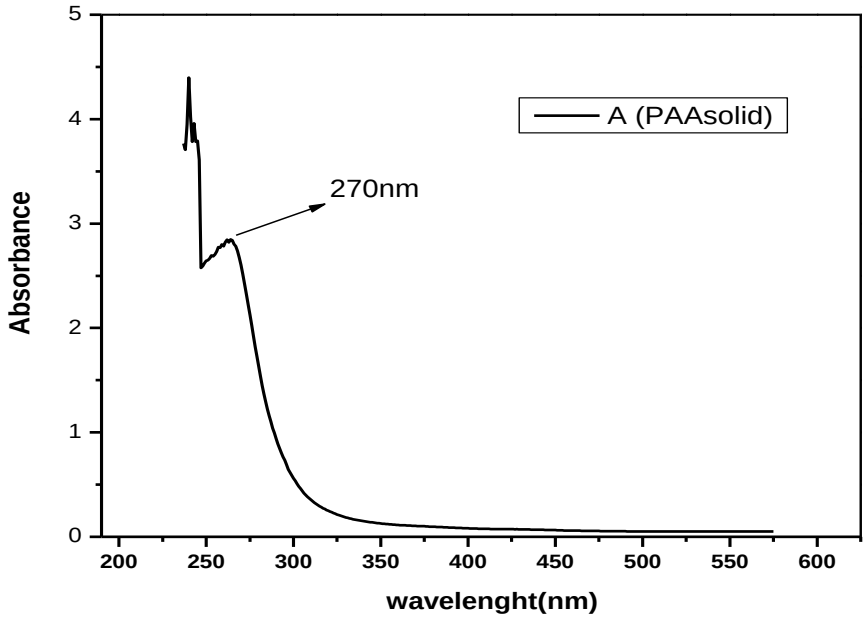

Figure 23: Ultra violet visible spectroscopy of Polyamic acid

Uv-vis characterisation of PAA was observed to have an absorption peak at 270nm which was attributed to amine group in PAA (figure 23). The band gap energy of the polyamic acid was found to be 4.58 eV equivalents to 7.34 x10^{-19} J, calculated using the equation 3.

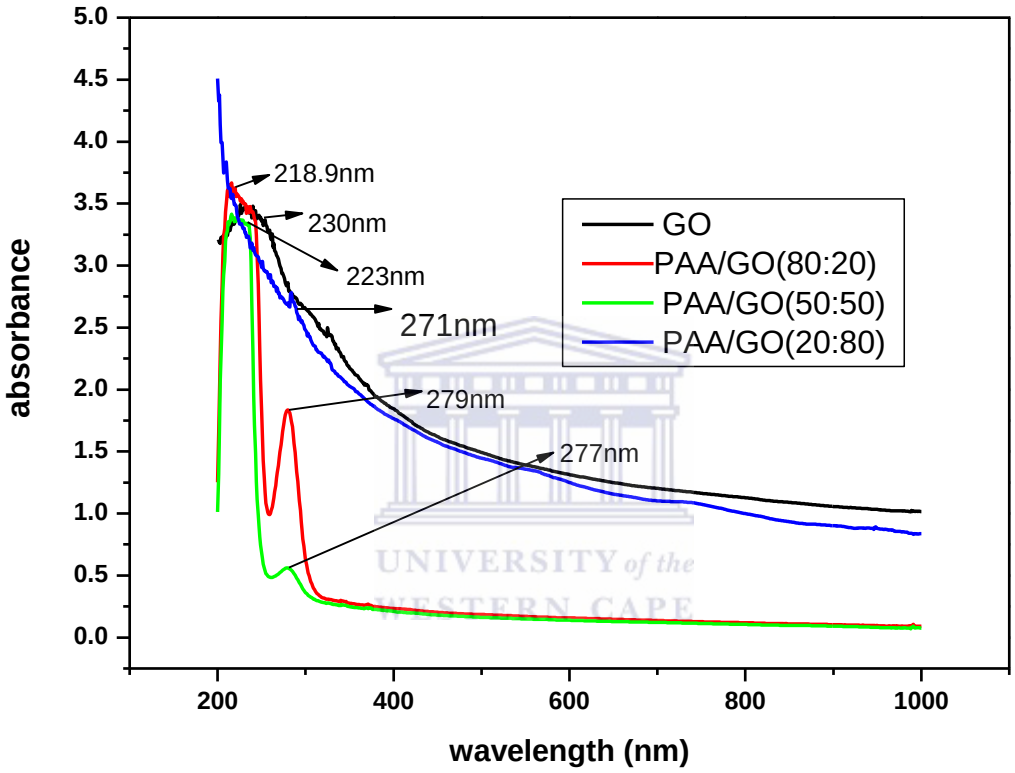

Figure 24: Ultra violet visible spectroscopy of composite material

The absorption spectrum of GO: PAA (50:50) and PAA: GO (80:20) clearly showed the presence of PAA as a proportional peak at 270 nm. This peak was absent in the GO: PA (80:20) spectrum when graphene oxide was the dominant component (figure 24).

Table4: Uv-vis absorption wavelength

Materials	Band gap (eV)	Band gap in (J)	Absorption wavelength(nm)
PAA	4.48	$7.34x10^{-19}$	270nm
GO	5.37	$8.61x10^{-19}$	230nm
PAA: GO(50:50)	5.54, 5.45	$8.88x10^{-19}$, $8.73x10^{-19}$	223nm, 277nm
PAA: GO(80:20)	5.67, 4.43	$9.09x10^{-19}$. $7.10x10^{-19}$	218nm, 279nm
PAA: GO(20:80)	4.56	$7.31x10^{-19}$	271nm

4.3 Electrochemistry of the newly formation composites

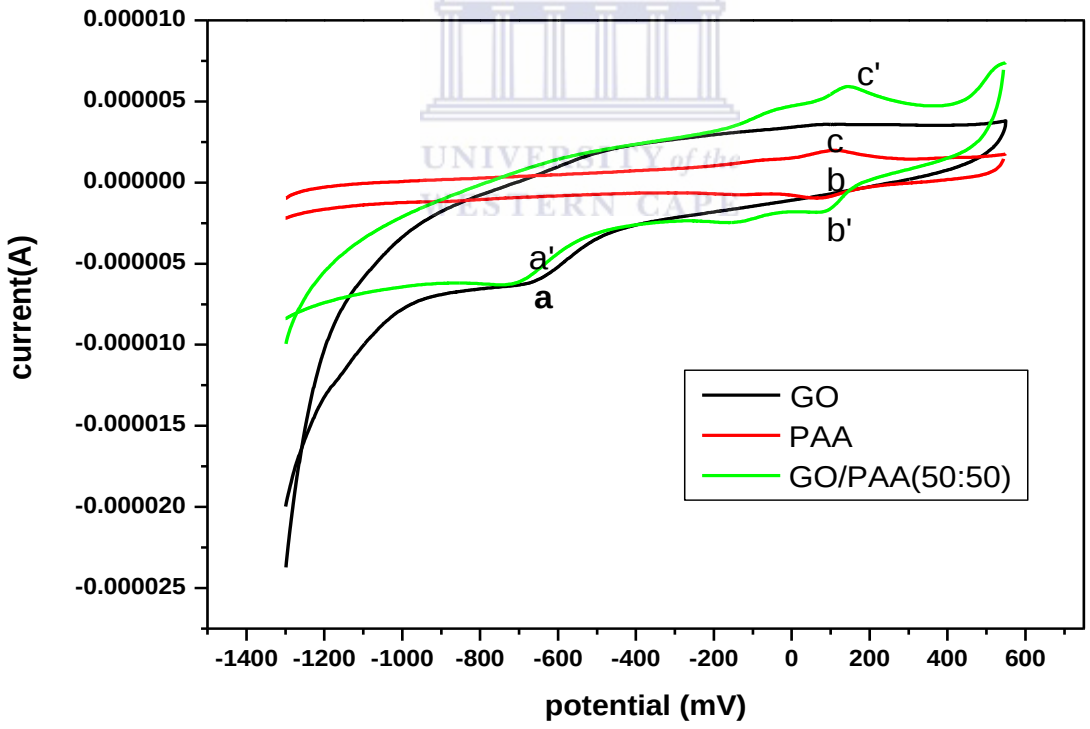

Figure 25: Cyclic voltammetry of GO, PAA and GCE/PAA: GO (50:50) in phosphate buffer pH 7.3 at 60mVs^{-1}.

The CV of PAA: GO (50:50) showed overlapping peaks, at -653.8 mV which was evident of graphene oxide. The peaks at 75.0 mV and 145.6 mV were evident of amine electrochemistry from PAA (figure 25). The peaks denoted a, b and c was assigned to GO whereas a'', b'' and c'' were assigned to GO: PAA composite. Electrochemical signature of the electro-synthesised composites compared to graphene oxide and polyamic acid on the electrode was visibly different.

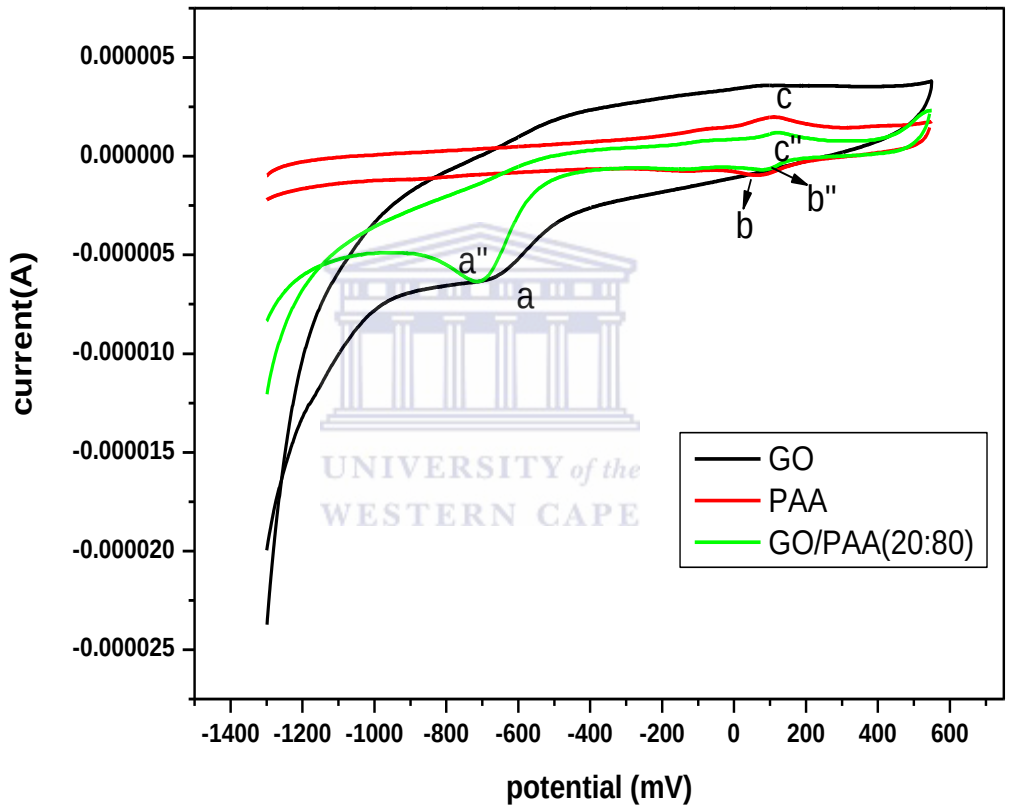

Figure 26: Cyclic voltammetry of GO, PAA and GCE/ PAA: GO (80:20) in phosphate buffer pH7.3 at 60mVs^{-1}.

The peaks identified in the composite PAA: GO (80:20) overlapped with peaks in starting materials providing evidence that the composite deposited included electrochemistry of both the starting materials. The diffusion coefficient was calculated from the peak response as -646.2 mV (a'') and 121.04 mV (c'') where increased peak current with increase in scan rate

was observed.

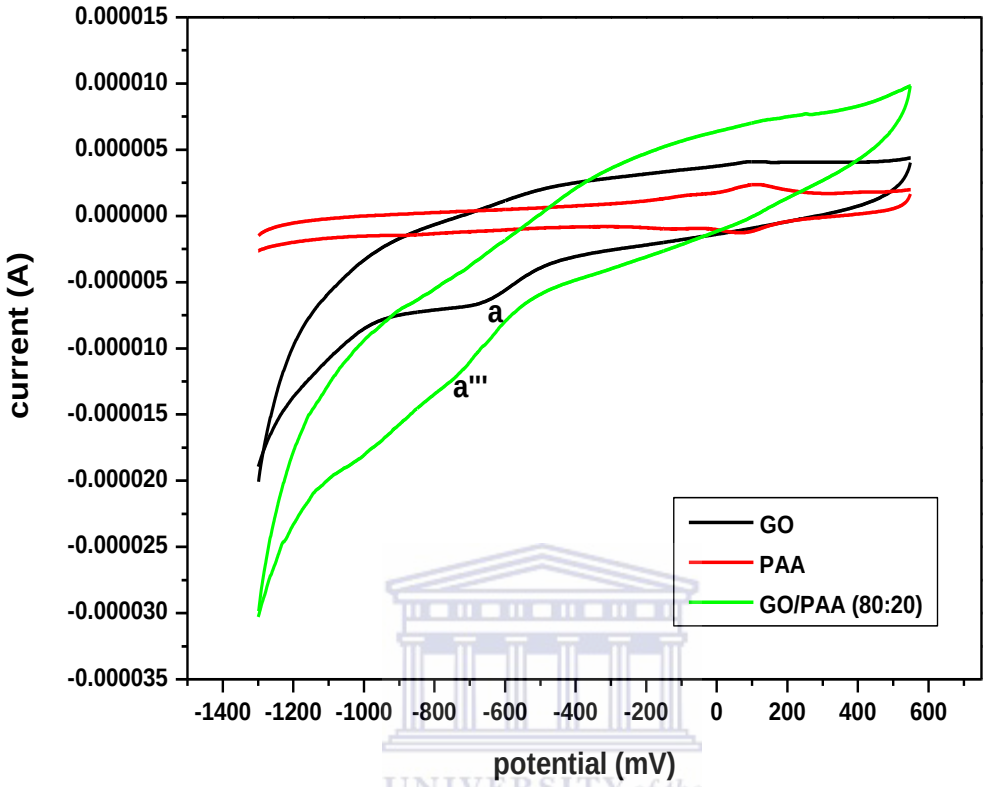

Figure 27: Cyclic voltammetry of GO, PAA and PAA: GO (20:80) in phosphate buffer pH7.3 at 60 mVs^{-1}

The cyclic voltammetry revealed that the graphene oxide has a reduction peak at about -650 mV which is due to the oxygen functionality (figure 27). GO contains oxygen functional groups, such as epoxides, −OH, and −COOH groups. Also reduction and oxidation peak appearing at +120mV and -182mV which is due to the amine group from the structure of polyamic acid. When we compared the cyclic voltammetry GO: PAA (80:20) the GO electrochemistry was observed as the dominant peak in the cyclic voltammetry, but evidence of PAA redox couple could still be observed.

For reversible reaction, the concentration is related to peak current by the Randles-Sevcik Equation (at 25 °C), (Equation 4) and for irreversible reaction (Equation 10)

$$Ipc = (2.99\times10^{5})\, n\, (\alpha na)\, A\, Co^{*} D\, o^{1/2}\, V^{1/2} \qquad \text{(Equation 10)}$$

Where Ip = Peak Current, n =one is the number of electrons involved in the reaction, A = 0.071 cm^2 is the geometric area of the electrode, D is the diffusion coefficient (cm^2 s^{-1}). Ipc is peak cathodic current and Ipa is the peak anodic current, Co is the concentration in $mol.cm^{-3}$ or Concentration of bulk substrate concentration and V = scan rate in V s^{-1}. Representative plots were obtain for 50:50 (figure 28), 80:20 (figure 29) and 20:80 (figure 30) nanocomposites cyclic voltammetry.

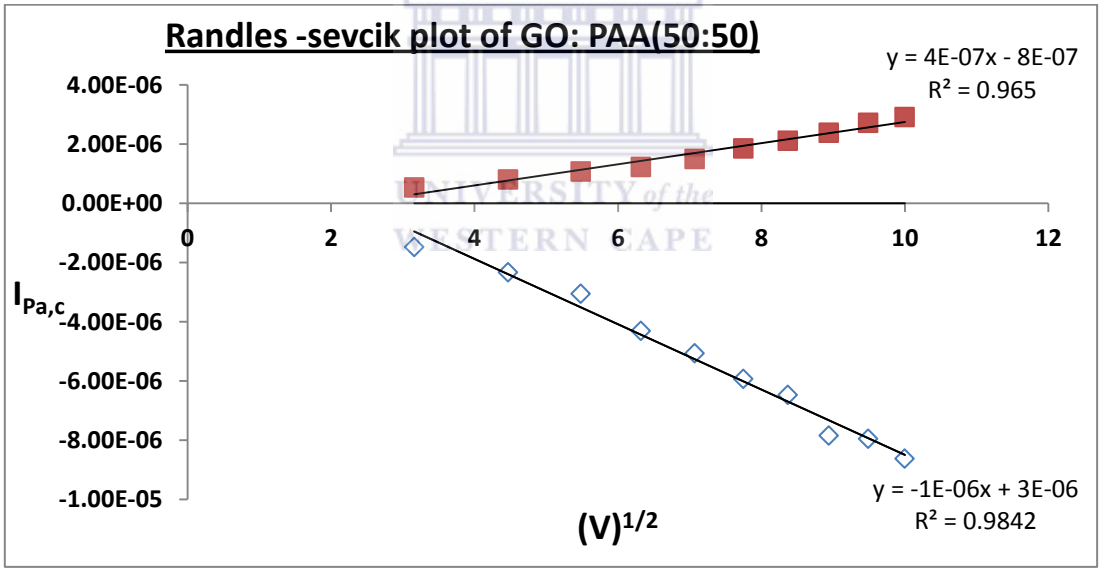

Figure 28: Randles -Sevcik plot of peak current vs. square root of the scan rate for PAA: GO (50:50) in PBS, at scan rates 10 – 100 mVs^{-1}

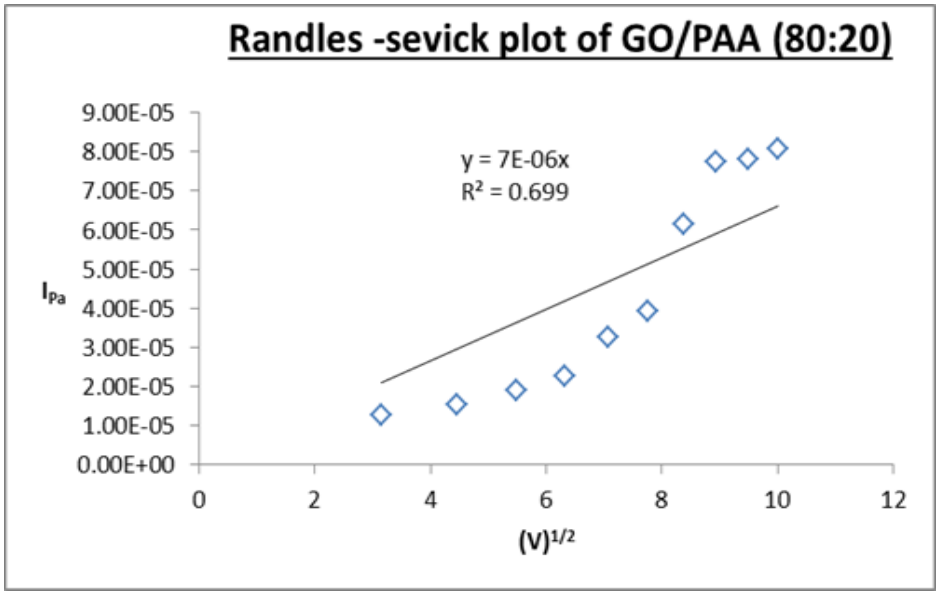

Figure 29: Randles- Sevcik plot of peak current vs. square root of the scan rate for PAA: GO (80:20) in PBS, at scan rates 10 – 100 mVs^{-1}

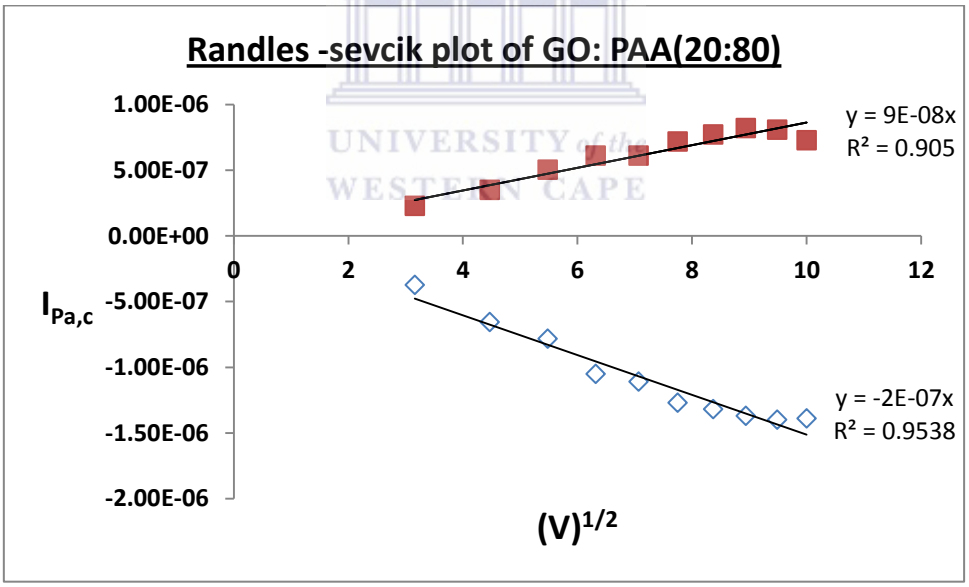

Figure 30: Randles- Sevcik plot of peak current vs. square root of the scan rate for PAA: GO (50:50) in PBS, at scan rates 10 – 100 mVs^{-1}

Table 5: Diffusion coefficient and slope obtained from the Randles Sevcik plots for PAA: GO nanocomposites.

materials	Peaks of the materials	Slope (A/mVs^{-1})	Diffusion Coefficient (cm^2s^{-1})	Regression Coefficient (R^2)	E^{0-} (1) (mV)	E^{0-} (2) (mV)
GO	peak **(a)**	5×10^{-7}	1.072×10^{-6}	0.933	-	-
PAA	peak **(c)**	4×10^{-7}	1.75×10^{-11}	0.983	87.75	85.80
	peak **(b)**	7×10^{-7}	5.37×10^{-11}	0.992		
PAA: GO (50:50)	peak **(c´)**	4×10^{-7}	2.46×10^{-14}	0.965	110.37	94.96
	peak (**a´**)	1×10^{-6}	1.754×10^{-13}	0.984	-	-
PAA: GO (80:20)	Peak **(c´´)**	9×10^{-8}	1.096×10^{-14}	0.905	94.92	-
	Peak **(a´´)**	2×10^{-7}	2.221×10^{-15}	0.953	-	-
PAA: GO (20:80)	Peak **(a´´´)**	7×10^{-6}	1.343×10^{-11}	0.699	-	-

*

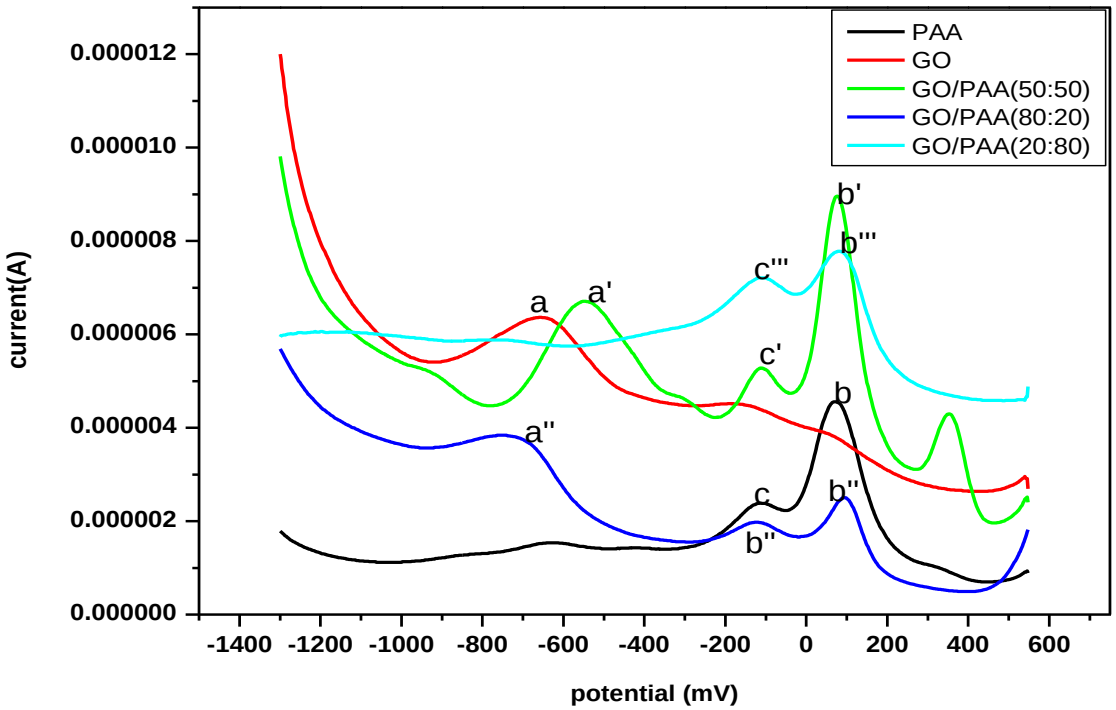

Figure 31: Reduction square waves of GCE-PAA: GO at different ratios in phosphate buffer saline pH7.3 at scan rate of 30mVs^{-1}; potential range between -550 and 1300mV (3M NaCl).

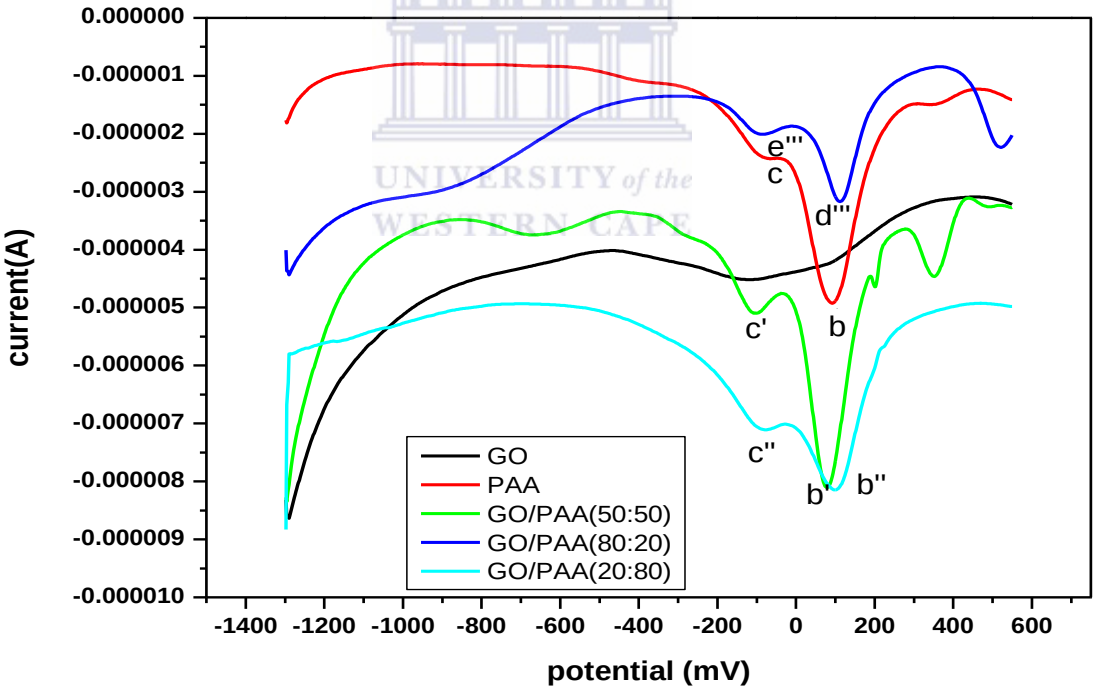

Figure 32: Oxidation square waves of GCE/PAA: GO at different ratios in phosphate buffer saline pH7.3 at scan rate of 30mVs^{-1}; potential range between -550 and 1300mV (3M NaCl)

The in-situ electrochemical synthesis of PAA: GO composites onto the glassy carbon an electrode was studied at different mole ratio of PAA and GO, under potentiodynamic conditions. The different composite films obtained were characterized by different shapes of peak position. The data from each individual SWV plots of the different composites have been extracted and is summarised in Table 6, thus the individual square wave voltammetry of each composite are shown as well as their formal potential.

Table6: Formal potential from the Square wave voltammetry for PAA: GO onto glassy carbon electrode in 0.1M PSB.

materials	Peaks of materials	cathodic peak potential(mV)	anodic peak potential(mV)	Formal potential(mV)
GO	Peak **a**	-667.9	-	-
PAA	Peak **b**	79.09	96.02	87.55
PAA	Peak **c**	-130.24	-102.02	116.13
PAA: GO (50:50)	Peak **a´**	-540.93	-	-
	Peak **b´**	89.20	81.90	89.20
	Peak **c´**	-130.13	-116.13	116.13
PAA: GO (80:20)	Peak **a´´**	-724.86	-	-
	Peak **b´´**	89.20	110.62	99.91
	Peak **c´´**	-130.24	-102.02	116.01-
PAA: GO (20:80)	Peak **a´´´**	-	-	-
	Peak **b´´´**	81.90	110.62	96.26
	Peak **c´´´**	-122.95	-87.91	105.43

To obtain formal potential above it was obtain using the following equation

$$E^{o} = \frac{pa+pc}{2} \qquad \text{(Equation 11)}$$

From the data obtained from square wave voltammogram of the different ratios of PAA: GO composites it is evident that as the amount of PAA increases the peak potentials (Epa and Epc) shift to more positive values. Peak **b** and **c** of polyamic acid is dominant for all composites in both reduction and oxidation peak.

CHAPTER 5

This biosensor response to microcystin-LR in solution will be reported here. The biosensor response was evaluated by cyclic voltammetry, Square wave voltammetry, electrochemical impedance spectroscopy and ultra violet visible spectroscopy. Details of enzyme linked immunosorbent-assay for the determination of spiked samples will be provided.

5.1. Electrochemistry of biosensor

5.1.1 Electrochemical response PP2a to microcystin-LR

The electrochemical response of immobilised PP2a was measured as the corresponding oxidation current to concurrent increase in microcystin-LR concentration. First the PP2a was immobilised in the glassy carbon electrode directly to separate the enzyme response from the modified platform electrochemistry. Secondly the biosensor was constructed by modifying the glassy carbon electrode with GO: PAA (50:50) and then immobilising the PP2a at the modified interface.

Concentration dependent analysis of microcystin was performed at GCE/PP2a to observe the response redox chemistry and analytical signal of immobilised PP2A towards MC-LR in solution. The electrochemical window used was -1300 mV and 550 mV and scan rate of 100mVs^{-1} in PBS (pH7.4). A single irreversible reduction peak was observed at -860 mV which showed a consecutive increase with each addition of microcystin-LR (figure 33). The current response was linear in the concentration range used, with a R^2 = 0.99146 with sensitivity was calculated from the slope of the linear regression line as 1.48452 x 10^{-6}A.nM^{-1} (figure 34).The limit of detection (0.51nM) was calculated using the following equation:

$$D_L=\frac{3 \text{ x } SD}{slope} \qquad \text{(Equation 12)}$$

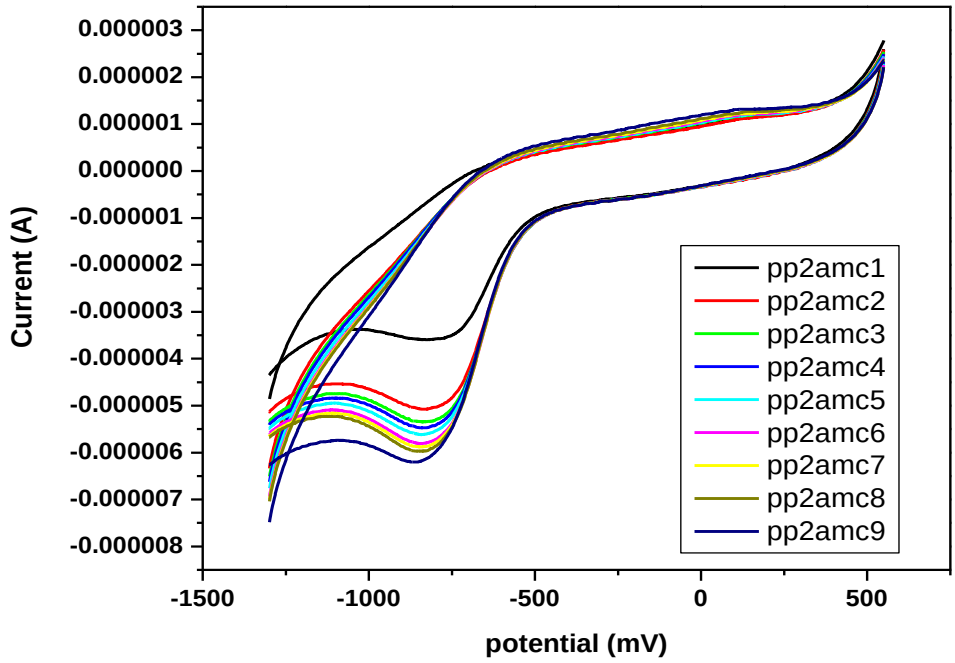

Figure 33: Cyclic voltammetry of GCE/PP2a microcystin-LR in PBS (pH=7.4)

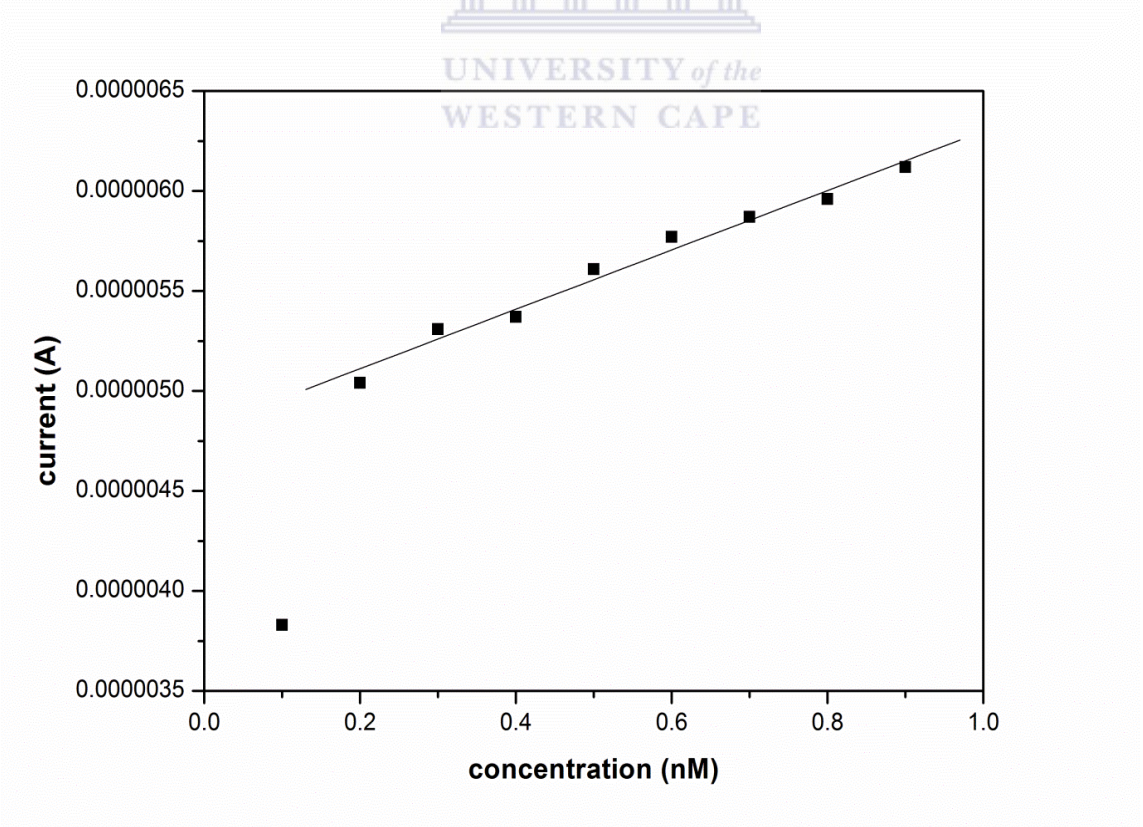

Figure 34: Calibration curve of GCE/PP2A in the presence of microcystin-LR

The electrochemical response of the GCE/PAA: GO-PP2a biosensor was evaluated using the same parameters as in the previous experiment. The redox couple at E° = 214 mV was assigned to the electrochemistry of the PAA: GO and was observed to be well separated from the biosensor analytical peak at -860 mV which showed a similar increase to microcystin-LR concentration as before (figure 35). The current response was observed to be linear in the concentration range used, with a R^2 =0.9735 with a sensitivity of 4.5 x 10^{-7} A.nM^{-1} and a limit of detection of 0.67 nM (figure 36).

From literature it is well known that SWV has higher sensitivity for redox chemistry compared to CV. Hence the calibration curve for the biosensor response to microcystin-LR was also evaluated from reduction square wave, complimenting the CV experiment. However, the sensitivity (1.4 x 10^{-7} A/mol^{-1}) and limit of detection (1.2 nM) was found to be comparable to the values obtained from CV (figure 37). This confirmed that the biosensor sensitivity was inherent to the bio-recognition event and not much affected by the voltammetry method employed.

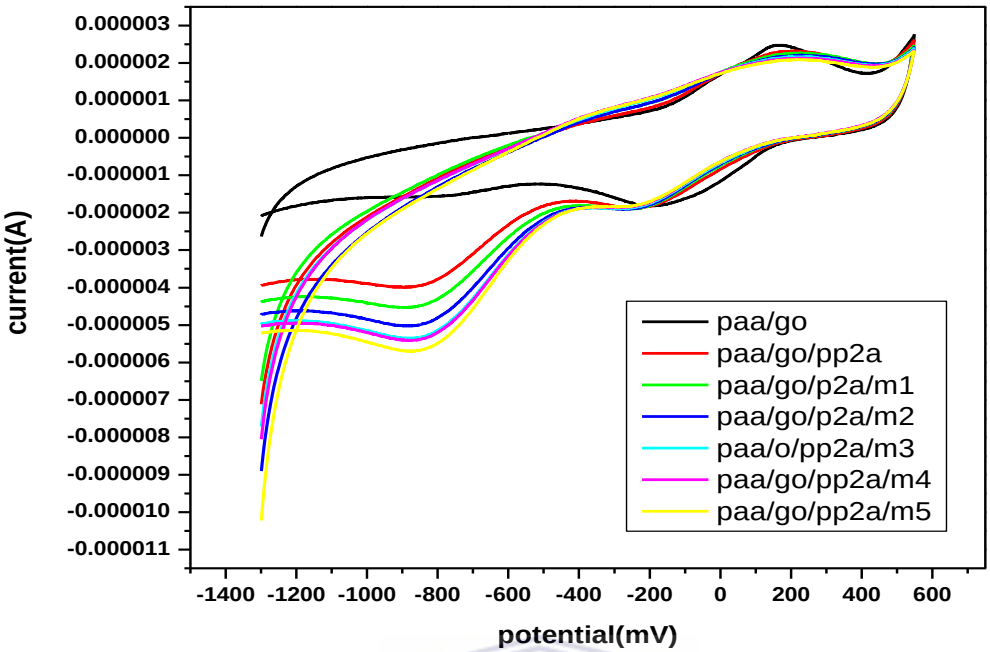

Figure 35: Cyclic voltammetry responses of GCE/PAA: GO-PP2a biosensor to different concentrations of microcystin-LR in 0.1M PBS saline (pH=7.4).

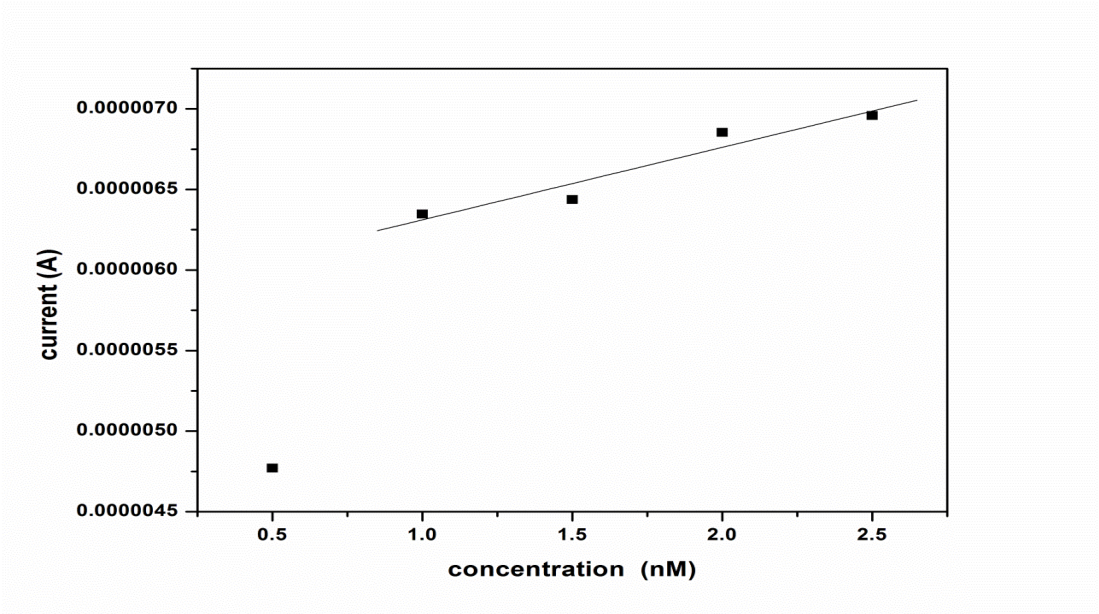

Figure 36: Calibration curve for GCE/PAA: GO-PP2a biosensor CV response to microcystin-LR

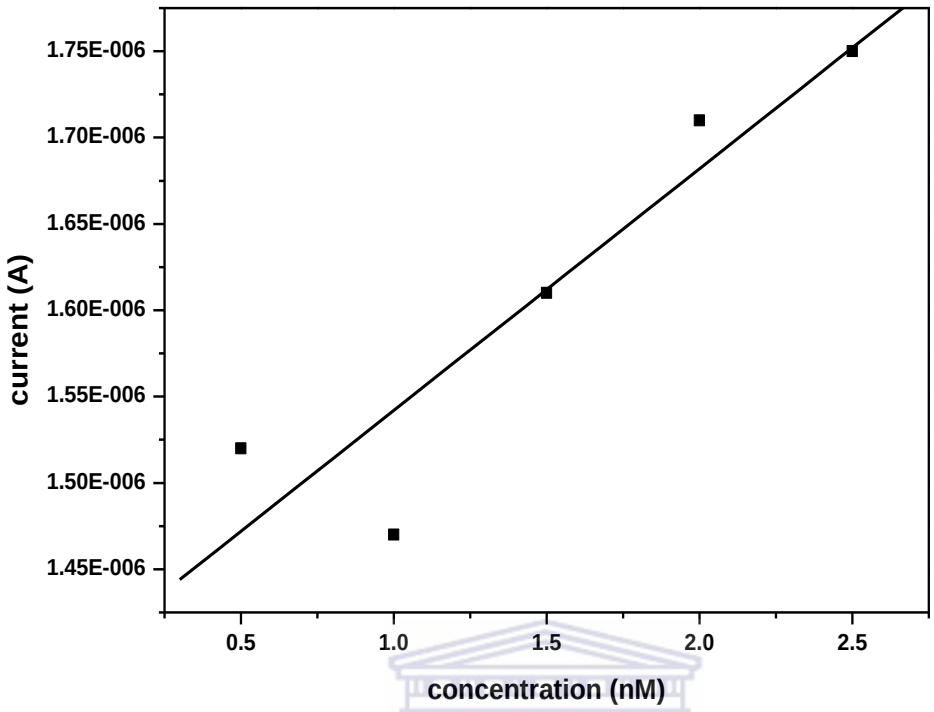

Figure 37: Calibration curve for GCE/ PAA: GO-PP2a biosensor response to microcystin-LR obtained from square wave voltammetry

5.1.2 Characterizations of the biosensor using electrochemical impedance spectroscopy (EIS)

The impedance data collected at 100 mV intervals over a potential range from 100 – 500 mV to confirm the integrity of the analytical peak potential chosen. The peak at 214 mV also showed a peak current response to concentration of microcystin-LR, when evaluated by SWV. The data was -modeled as a Randles equivalent circuit and the Rct values extracted for the fitting of the EIS data (figure 38).

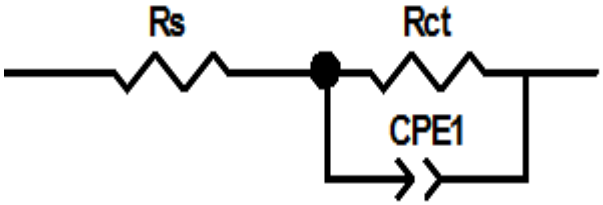

Figure 38: Randles circuit used for data fitting

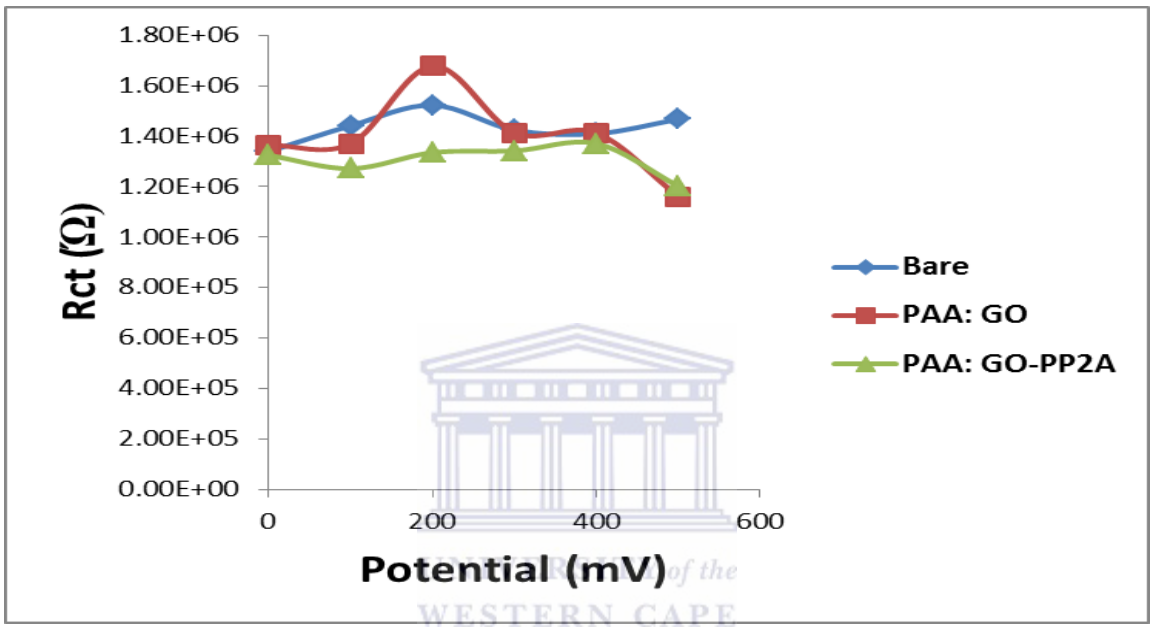

Figure 39: Charge transfer resistance vs. potential for the modification steps in biosensor design.

The Rct values peaked at 200 mV for the PAA: GO composite as compared to bare GCE and biosensor, confirming that the redox couple observed was unique to the PAA: GO platform. The couple only observed in SWV voltammetry due to the improved sensitivity of the technique to Faradaic processes. The biosensor response to microcystin-LR were monitored at -810 mV (vs. Ag/AgCl) as before in voltammetry analysis (figure 40) .The calibration curve based on Rct as a function of increasing microcystin-LR concentration was evaluated for the biosensor response parameters (figure 41).

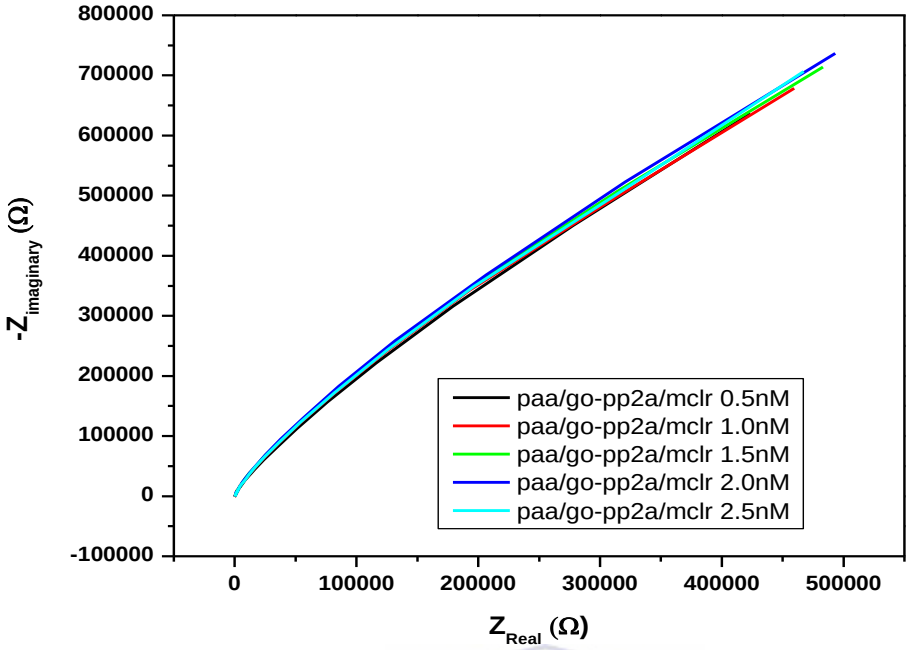

Figure 40: Nyquist plot biosensor response to microcystin-LR.

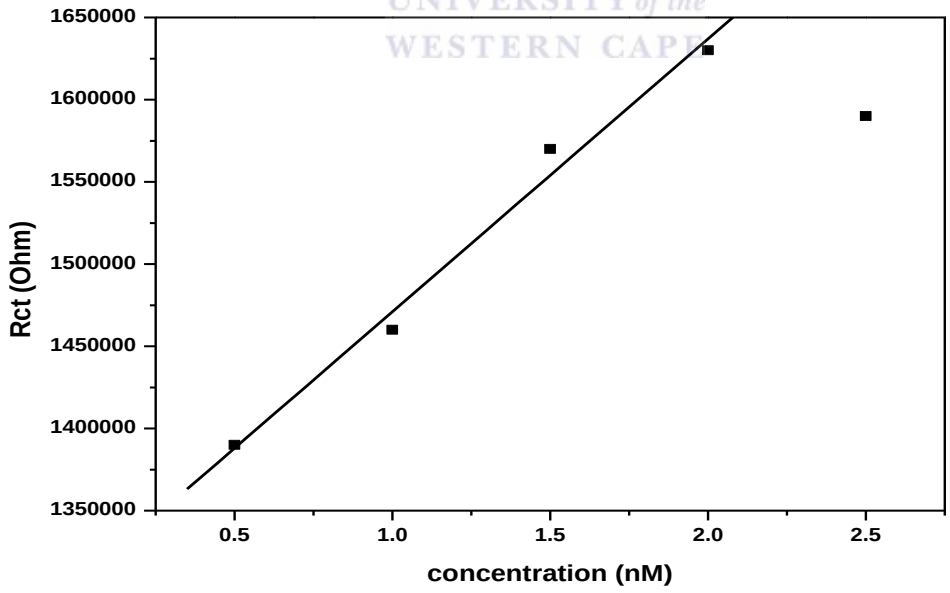

Figure 41: Resistance vs. concentration of PAA: GO-PP2a biosensor to microcystin-LR at a fixed potential (250mV)

Using the same concentration range as in voltammetry experiments the sensitivity of the biosensor was obtained from the slope of the calibration curve (16600 $OhmnM^{-1}$) and the detection limit was calculated as 2.65 nM. In all three methods used to quantify the biosensor performance parameters, it was evident that the biosensor constructed in this work, had much higher sensitivity towards microcystin-LR and very low detection limit. The performance of the biosensor was significantly higher when compared to ELISA, HPLC-UV and LC-MS methods (Spoof et al., 2003) which have detection limit of $0.2\mu gl^{-1}$. This improved sensitivity was assigned to good orientation of the enzyme on the novel platform designed during immobilisation step, retention of the integrity of the enzyme during immobilisation, good compatibility with the novel PAA: GO platform and the high affinity of the PP2a for microcystin-LR.

5.1.3 Uv-vis of microcystin-LR and PP2a interaction

The binding of PP2a to microcystin-LR when both components dispersed in the same solution, was evaluated using Uv-vis spectroscopy. 10µl of PP2a dissolved in PBS buffer, to which different concentration of microcystin-LR were added. The absorption peak at 250 nm identified as the analytical signal and the concentration response evaluated as the relevant calibration curve.

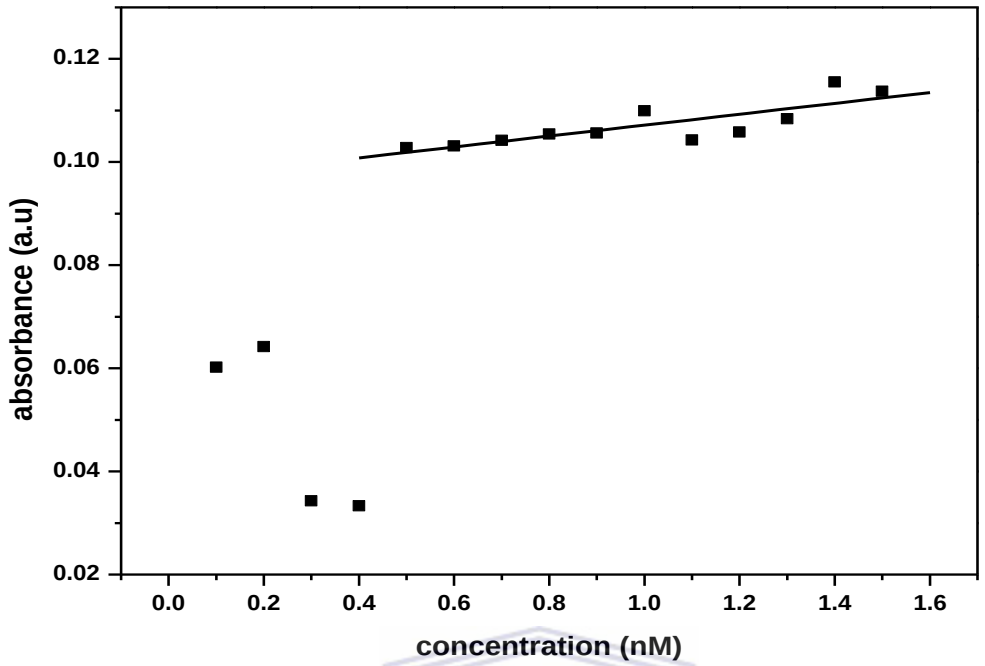

Figure 42: UV- Vis absorbance spectroscopy for the binding of microcystin with PP2a in PBS solution.

The spectra presented an absorption peak at 250nm which showed an increasing trend upon additions of microcystin-LR. At lower concentration (0.1 - 0.4 nm) a linear increase in absorbance was observed but as the concentration was increased above 0.4 nM, the absorption intensity started to fluctuate. The PP2a enzyme showed sensitivity to microcystin-LR in solution of 0.049 a.u.nM^{-1} with a detection limit 0.28 nM.

5.1.4 Enzyme linked immunoassay (ELISA)

The detection of microcystin-LR was done using standard ELISA Abraxis kit. Wastewater was taken from scientific services City of Cape Town, tap water from our laboratory and distilled water. Following the ELISA protocol, the standard solutions of the Abraxis kit showed an inverse relationship between concentration and absorbance i.e.as absorbance decreased concentration increased (figure 44).

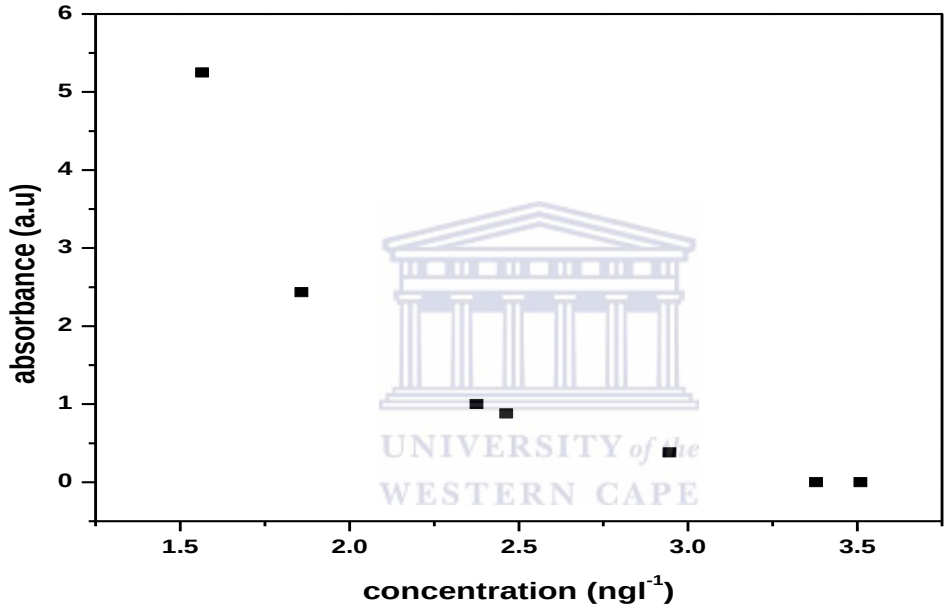

Figure 43: Calibration curve of microcystin-LR standards from the ELISA kit

An attempt was made to prepare real water samples by spiking with microcystin-LR and recovery measurement by ELISA method. Diluted standards to compare with the low concentration range where the biosensor was able to measure (0.5-2 ngl^{-1}), was prepared (table 7). However, after ELISA treatment, these standards gave absorbance readings that were off the high end of the absorbance scale (figure 45). The three samples selected i.e. tap water, distilled water and a random wastewater sample (provided by City of Cape Town water treatment laboratory, gave extremely low absorbance readings (<1 a.u).

Table 7 Attempted real samples analysis by ELISA method

Concentration (ngl^{-1})	Absorbance (a.u)	Sample
-	0	Distilled water
-	0.12	Tap water
-	0.313	Waste water
0.5	5.25	MC-LR standards 1
1.0	5.25	MC-LR standards 2
1.5	5.25	MC-LR standards 3
2.0	5.25	MC-LR standards 4

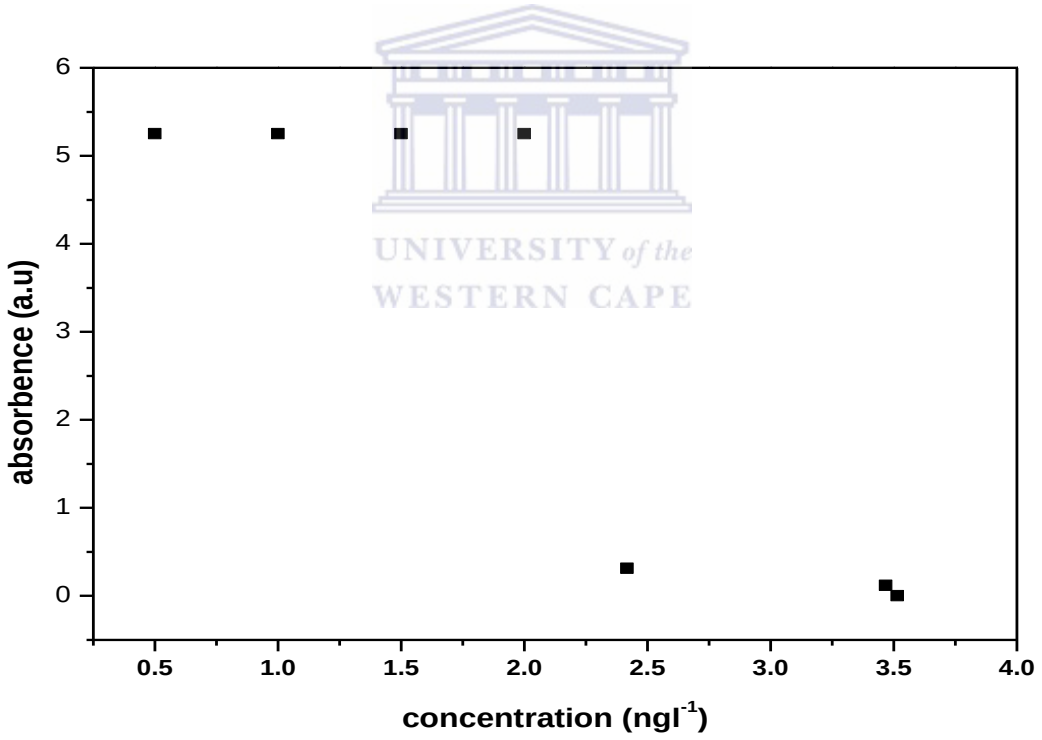

Figure 44: Absorbance profile of real water samples compared to diluted standards prepared.

This served as confirmation that the ELISA method worked well for concentration at the higher end of the microcystin-LR concentration range. The advantage and potential usefulness of the novel biosensor prepared lies in very low detection capability, which could be employed for early detection of algal blooms and early warning signalling of potential algal bloom events. In this work no direct correlation could be drawn between the concentration range employed in the biosensor analysis and the concentration capability of the ELISA method employed.

CHAPTER 6

Conclusions

Graphene was chemically synthesized from graphene oxide using Hummer's method. Polyamic acid was synthesized chemically as a yellow powder from ODA and PMDA. The first objective of the research was to produce novel PAA:GO nanocomposites by electrochemical polymerisation method. Electropolymerisation produces in situ nanocomposites, when the deposition of material is controlled by physical parameters (electrode surface area, deposition rate, solubility etc.) as well as chemical parameters (concentration of polymers, solubility, pH, buffers, solvents etc.).

A progression of new polyamic acid and graphene oxide (PAA: GO) composites were electrochemically synthesized in-situ and characterized in 0.1 M phosphate buffer solutions at pH of 7.3. Evidence provided by CV, SWV, Uv/vis spectroscopy, SEM and AFM confirm that the GO and PAA have combined to form new, uniformly dispersed polymer composite thin films. The composition of the films were controlled by starting material ratio and scan rate to produced electro-active thin films with a unique electrochemical signature and diffusion controlled electro kinetics (De), under potentiodynamic control. The morphology of the composites echoed the morphology observed for the dominant polymer in the synthesis mixture. The structural analysis of the composites by spectroscopic methods (Uv-vis absorption and FTIR spectroscopy) confirmed the presence of GO and PAA functionality in the final composites. The electrochemical evaluation (CV, SWV) confirmed that the functional group electrochemistry if the starting polymers were retained in the final nanocomposites produced as thin films at GCE electrodes.

A biosensor was constructed on the PAA:GO (50:50) composite platform, by immobilization of protein phosphate 2A by incubation method. The biosensor was applied for low level

detection of Microcystin LR. The microcyustin-LR was obtained as ELISA standards (Abraxis) and some elementary comparison between ELISA sensitivity towards microcystin-LR and the range of the biosensor was explored. The voltammetric studies produced strong analytical signal for measurement of microcystin-LR binding to immobilized to PP2A, as measured in phosphate buffer. The current response was linear in the nano molar concentration range used, with sensitivity to microcystin-LR 4.5 x 10^{-7} A/mol^{-1} and limit of detection 0.67 nM. The improved sensitivity was due to the conductive PAA:GO platform and the inherent sensitivity of protein phosphatase 2A towards microcystin-LR.

Future work

The application of the biosensor to real sample analysis will form the major focus area of future work. This will involve assessment of all three PAA:GO compositions as transducer platforms for enzyme immobilization, reproducibility of the biosensor response parameters, and optimization of repeatability of biosensor design and application in a multichannel array analysis framework. The multichannel array system will facilitate the in situ preparation of the biosensor platform, immobilisation of the enzyme and application to microcystin-LR analysis.

The biosensor performance will be compared thoroughly to ELISA capability for the same measurement, first working with simulated real samples produced by spiking with standard solution and recovering the microcystin-LR. Afterwards real samples will be attempted and profiled in collaboration with water treatment laboratories for trend analysis and investigation of biosensor as an early warning signaling system.

References

An, J. S., and Carmichael, W. W. 1994. Use of a colorimetric protein phosphatase inhibition assay and enzyme-linked-immunosorbent-assay for the study of microcystins and nodularins. Toxicon 32, 1495–1507.

Andreescu, D., Wanekaya, A.K., Sadik, O.A., Joseph Wang, J. 2005. Nanostructured Polyamic Acid Membranes as Novel Electrode Materials. Langmuir 21, 6891-6899.

Andrienko, D. 2008. Cyclic Voltammetry 22.

Armstrong Varsha Gupta, R.W., Ogawa, A.K., Du, X., Houk, K.N. 1997. A Model for Binding of Structurally Diverse Natural Product Inhibitors of Protein Phosphatases PP1 and PP2A. *Journal of Medicinal Chemistry* 40, 3199-3206.

Barford, D., Das, A.K., Egloff, M. 1998. The structure and mechanisms of protein phosphatase: Insights into Catalysis and Regulation. Bimolecular Structure 27, 133–164.

Barik, S., Kumar, R., Adams, B., Oldenburg, A., Musiyenko, A. 2002. Characterisation and expression of a PP1 serine/threonine protein phosphatase (PfPP1) from the malaria parasite, Plasmodium falciparum: demonstration of its essential role using RNA *interference. Malaria Journal* 1, 1-11.

Botha, A.M., Oberholster, P.J., Cloete, T.E. 2005. An overview of toxic freshwater cyanobacteria in South Africa with special reference to risk, impact and detection by molecular marker tools. *Biochemistry* 17(2), 57-71.

Brooks, W.P., Codd, G.A. 1988. Environmental Technology Letter. 9,1343.

Butler, E. J. 2000. Enzyme Linked Immunosorbent Assay. *Journal of Immunoassay* 21:2-3, 165-209.

Campas, M., Szydłowska, D., Trojanowicz, M., Marty, J. 2007. Enzyme inhibition-based biosensor for the electrochemical detection of microcystins in natural blooms of cyanobacteria. *Talanta* 72, 179–186.

Chamberlin, A.R., James E. Sheppeck, J.E., Gauss, C.M. 1997. Inhibition of the Ser-Thr Phosphatases PP1 and PP2A by Naturally Occurring Toxins. Bioorganic & Medicinal Chemistry, Vol. 5(9), 1739-1750.

Carmichael W.W.1997 The cyanotoxins.Advances in Botanical Research.vol 27, pp: 211–256

Chern, Y.T., Hua, M.Y., Chen, H.C., Chuang, C.K., Tsai, J.Y., Jeng, J.L., Yang, H.W. 2011. The intrinsic redox reactions of polyamic acid derivatives and their application in hydrogen peroxide sensor. *Biomaterials* l32, 4885-4895.

Chorus, I., Bartram, J. 1999. Toxic Cyanobacteria in Water: A guide to their public health consequences, monitoring and management. WHO.

Chow, C.W.K., Drikas, M., House, J., Burch, M.D. Velzeboer, R.M.A. 1999. The impact of conventional water treatment processes on cells of the cyanobacterium Microcystis aeruginosa. *Water Research* 33(15), 3253-3262.

Chu, F.S., Huang, X., Wei, R.D. 1990. *J. AOAC* .73, 451.

Cook, D., Newcombe, G. 2002. Removal of microcystin variants with powdered activated carbon. Water Science & Technology: Water Supply 2(5/6), 201-207.

Dukelow,M., Honkanen,R.E., Zwiller, J., Mooren, R.E., Daily, S.L., Khatrall, B.S., Boynton, A.L. 1990. Characterization of Microcystin- LR, a Potent Inhibitor of Type 1 and Type 2A Protein Phosphatases. *The journal of biological chemistry* 265, pp 19401-19404.

Figueiredoa, D.R., Azeiteirob, U.M., Estevesc, S.M., Goncalvesa,F. J.M., Pereiraa, M. J. 2004. Microcystin-producing blooms—a serious global public health issue. *Ecotoxicology and environmental safety* 59(2), pp 151-163

Fischer ,W. J., Garthwaite, I., Miles, C. O., Ross, K. M., Aggen, J. B., Chamberlin, A.R., Towers, R. N., and Dietrich, D. R.2001. Congener-Independent Immunoassay for Microcystins and Nodularins. *Environmental science and technology* 24, 4849-4856.

Fujiki1, H., Suganuma, M. 2011. Tumor Promoters - Microcystin-LR, Nodularin and TNF- α and Human Cancer Development. Anti-Cancer Agents in Medicinal Chemistry11, 4-18.

Gehringer, M.M. 2004. Microcystin-LR and Okadiac acid-induced cellular effects: a dualistic response. FEBS Letter 557, 1-8.

Gomez-Navarro, C., Sundaram, R.S., Balasubramanian, K., Burghard, M., Kern, K. 2008. Electrochemical Modification of Graphene. *Advanced Material* 20, 3050–3053.

Hart, J., Fawell, J. K., Croll, B. 1998. The fate of both intra- and extracellular toxins during drinking water treatment. *Water Supply* 16(1/2), 611-616.

Janssens, V., Gorisi, J. 2001. Protein phosphatase 2A: a highly regulated family of serine/ threonine phosphatases implicated in cell growth and signalling. *Biochemistry Journal* 353, 417-439.

Jones, G.J., Orr, P.T. 1994. Release and degradation of microcystin following algicide treatment of a Microcystis aeruginosa bloom in a recreational lake, as determined by HPLC and protein phosphatase inhibition assay. *Water Research* 28, 871–876.

Kakimoto, M., Yamanaka, K., Jikei, M. 2000. Preparation and Properties of Hyperbranched Aromatic Polyimides via Polyamic Acid Methyl Ester Precursors, 33, 6937-6944.

Lambert, T.W., Boland, M.P., Holmes, C.F.B., Hrudey, S.E. 1994. *Environmental. Science. Technology* 28, 753.

Landsberg, J.H. 2002. The effects of harmful algalblooms on aquatic organisms. Reviews in Fisheries Science 10, 113-390.

Lee, K.S., Kim, T.H., Shin, M.C., Lee, W.Y., Park, J.K. 1999. Disposable liposome immunosensor for theophylline combining an immunochromatographic membrane and a thick-film electrode. *Analytical. Electrochemica. Acta* 380, 17-26.

Li, Z., Shi, Y., Wu, J., Sun, Y., Zhang, Y., Wen, Z., Dai, H., Wang, H. 2012. A graphene oxide based biosensor for microcystins detection by fluorescence resonance energy transfer. *Biosensors and Bioelectronics* 38, 31-36.

Liu, C., Chen, L., Tang, Y., Luo, S. 2011. Direct electrode position of reduced graphene oxide on glassy carbon electrode and its electrochemical application. *Electrochemistry communications* 13, 133-137.

MacKintosh, C., Beattie, K.A., Klumpp, S., Cohen, P., Codd, G.A. 1990. Cyanobactrial microcystin-LR is a potent and specific inhibitor of protein phosphatase 1 and 2A from both mammals and higher Plants. *FEBS 08427*, 264, 187-192.

MacKintosh, C., MacKintosh, R.W., Codd, G.A., Jefferies, T.M., Kevil, C.W., Potters (Eds.), E. 1994. Detection Methods for Cyanobacterial Toxins, the Royal Society of Chemistry, Cambridge, 90.

Marzec, H.M., Krezel, A., Justyna Kobos, J., Plinski, M. 2006. Toxic Nodularia spumigena blooms in the coastal waters of the Gulf of Gdansk: a ten-year survey. Oceanologia 48 (2), 255–273.

McElhiney, J and Lawton, L.A. 2005. Detection of the cyanobacterial hepatotoxins microcystins. *Toxicology and applied pharmacology* 203, pp 219–230

Meriluotoa, J., Kincaidb, B., Smythb, M.R., Wasbergc, M. 1998. Electrochemical detection of microcystins, cyanobacterial peptide hepatotoxins, following high-performance liquid chromatography. *Journal of Chromatography* 810, 226–230.

Msagati, T.A.M., Siame, B.A., Shushu, D.D. 2006. Evaluation of methods for isolation, detection and quantification of cyanobacterial hepatotoxins: a review article. *Aquatic toxicology* 78, 382-397

Ndangili, P.M., Baker, P.G.L., Iwuoha, E.I. 2010. A potential masking approach in the detection of dopamine on 3-mercaptopropionic acid capped ZnSe quantum dots modified gold electrode in the presence of interferences. *Journal of Electroanalytical Chemistry* 643, 77-81.

Ndangili, P.N., Iwuoha, E., Baker, P.G.L. 2011. Impedimetric response of a lable free genosensor prepared on 3-mercaptopropionic acid capped gallium selenide nanocrystal modified electrode. *International Journal of electrochemical science,* vol 6, 1438 – 1453.

Nguyen, S.T., Stankovich, S., Dikin, D., Piner, R.D., Kohlhaas, K.A., Kleinhammes, A., Jiac, Y., Wu, Y., Ruoff, R.S. 2007. Synthesis of graphene-based nanosheets via chemical reduction of exfoliated graphite oxide. *Carbon* 45, 1558–1565.

Noah N.M.; Omole M.; Stern S.; Zhang S.; Sadik O.A; Hess E.H; Martinovic L.;, Baker P.G.L.; Iwuoha E.I. 2012**.** Conducting polyamic acid membranes for sensing and site-directed immobilization of proteins. *Analytical Biochemistry*, 428, 54–63.

Nxusani, E., Baker, P.G.L., Iwuoha, E. 2012. 3-mercaptopropionic acid capped Ga2Se3 nanocrystals-cyp3a4 biosensor for the determination of 17alpha-ethinylestradiol in water. *NanoHybrids*, vol 1, 1-22.

Nxusani, E., Ndangili, P.M., Olowu, R.A., Jijana, A.N., Waryo, T., Jahed, N., Ajayi, R.F., Baker, P., Iwuoha, E. 2012. 3-Mercaptopropionic acid capped Ga2Se3 nanocrystal-CYP3A4 biosensor for the determination of 17alpha-ethinylestradiol in water. *Nano Hybrids* 1, 1-22.

Ozsoz, M., Erdem, A., Kerman, K., Meric, B., Ozkan, D., Kara, P. 2002. DNA Biosensor for Microcystis spp. Sequence Detection by Using Methylene Blue and Ruthenium Complex as Electrochemical Hybridization Labels. Turk J Chem 26, 851- 862.

Queirós, R.B., Noronha, J.P., Marques, P.V.S., Sales, M.G.F. Emerging (Bio) Sensing Technology for Assessing and Monitoring Freshwater Contamination – Methods and Applications.

Rapala, J., Erkomaaa, K., Kukkonen, J., Sivonen, K., Lahti, K. 2002. Detection of microcystins with protein phosphatase inhibition assay, high-performance liquid chromatography–UV detection and enzyme-linked immunosorbent assay Comparison of methods. *Analytica ElectroChimica Acta* 466, 213–231.

Robert W. Armstrong, Varsha Gupta, Anthony K. Ogawa, Xiaohui Du, and K. N. Houk. 1997. A Model for Binding of Structurally Diverse Natural Product Inhibitors of Protein Phosphatases PP1 and PP2A. *Journal of Medicinal Chemistry*, Vol. 40, 3199-3206.

Rubiolo, J.A., Lopez-Alonso, H., Alfonso, A., Vega, F.V., Vieytes, M.R., Botana, L.M. 2012. Characterization and Activity Determination of the Human Protein Phosphatase 2A Catalytic Subunit α Expressed in Insect Larvae. *Applied Biochem Biotechnology* 167, 918–928.

Ruoff, R.S., Dreyer, D.R., a Sungjin Park., Bielawski, C.W. 2010. The chemistry of graphene oxide. *Chemical society*, vol 39, 228–240.

Sadik, O.A., Du, N., Wong, C., Feurstein, M. 2010. Flexible Poly (amic -acid) Conducting Polymers: Effect of Chemical Composition on Structural, Electrochemical, and Mechanical Properties. *Langmuir* 26(17), 14194–14202.

Sadik, O.A., Mwilu, S.K., Aluoch, A. 2009. Smart electrochemical biosensors: From advanced materials to ultrasensitive devices. *Electrochimica Acta* 59, 4287–4295.

Sadik, O.A., Noah, N.M., Omole, M., S. Stern, S., Zhang, S., Hess, E.H., Martinovic, J., Baker, P.G.L., E.I. Iwoaha, E.I. 2012. Conducting polyamic acid membranes for sensing and site-directed immobilization of proteins. *Analytical biochemistry* 428, 54-63.

Sadik, O.A., Noah, N.M., Omole, M., Sterna, S., Zhang, S., Hess, E.H., Martinovic, J., Baker, P.G.L., Iwuoha, E.I. 2012. Analytical Biochemistry 428, 54–63.

Sadik, O.A., Yan, F., Ozsoz, M. 2000. Electrochemical and conformational studies of microcystin–LR. *Analytica Chimica Acta* 409, 247–255.

Siegll, G., MacKintosh, C., Stitt, M. Sucrose-phosphate synthase is dephosphorylated by protein phosphatase2A in spinach leaves 270, number 1, 2, 198-202.

Singh, A.K., Kilatrick, P.K., Carbonell, R.G. 1995. Noncompatitive immunoassay using bifunctional unilamellar vesicles or liposomes, *Biotechnology. Proy* 11, 333-341.

Singh, B.P., Singh, D., Mathur, R.B., Dhami, T.L. 2008. Influence of Surface Modified MWCNTs on the Mechanical, Electrical and Thermal Properties of Polyimide Nanocomposites. *NANO EXPRESS* 3, 444–453.

Sivonen, K., Siren, H., Jussila, M., Liu, H., Peltoniemi, S., Riekkola, M.-L.1999.Separation, purity testing and identification of cyanobacterial hepatotoxins with capillary electrophoresis and electrospray mass spectrometry. Journal Chromatography 839, pp. 203–215

Strack, S., Westphal, R.S., Colbran, R.J., Ebner, F.F., Wadzinski, B.E. 1997. Protein serinerthreonine phosphatase 1 and 2A associate with and dephosphorylate neurofilaments. *Molecular Brain Research* 49, 15–28.

Spoof, L.,Vesterkvista, Pia. Lindholmb, T., Meriluotoa, J. 2003. Screening for cyanobacterial hepatotoxins, microcystins and nodularin in environmental water samples by reversed-phase liquid chromatography–electrospray ionisation mass spectrometry. *Journal of chromatography A* 1020(1), pp 105-119.

Thema, F.T., Moloto, M.J., Dikio, E.D., Nyangiwe, N.N., Kotsedi, L., Maaza, M., Khenfouch, M. 2013. Synthesis and characterization of graphene thin films by chemical reduction of exfoliated and intercalated graphite oxide. *Journal of Chemistry,* 1-6.

Wang, C., Chao, D., Zhang, J., Liu, X., Lu, X., Zhang, W., Wei, Y. 2010. Synthesis of novel poly (amic acid) and polyimide with oligoaniline in the main chain and their thermal, electrochemical, and dielectric properties. Polymer 15, 4518-4524.

World health organisation, Toxic Cyanobacteria in Water. 1999. A guide to their public health consequences, monitoring and management.

www.epa.gov/gmpo/habpage.html

www.piercenet.com/method/protease-phosphatase-inhibitors

www.tms.org/pubs/journals/JOM/0010/Kumar/Kumar-0010.html

Yanga, K.S., Edieb, D.D., Limc, D.Y., Kimd, Y.M., Choia, Y.O. 2003. Preparation of carbon fiber web from electrostatic spinning of PMDA-ODA poly (amic acid) solution. *Carbon* 41, 2039–2046.

Ye, M., Shen, J., Hu, Y., Shi, Min., Lu, X., Li, C. 2009. Fast and Facile Preparation of Graphene Oxide and Reduced Graphene Oxide Nanoplatelets 21, 3514-3520.

Yongchao, Si. Edward T. Samulski. 2008. Synthesis of Water Soluble Graphene. Nano Letters 8 6), 1679-1682

Yoshizawa, S., Matsushima, R., Watanabe, M.F., Harada, K., Ichihara, A., Carmichael, W.W., Fujiki, H. 1990. Inhibition of protein phosphatases by microcystis and nodularin associated with hepatotoxicity. *Cancer research clinical oncology* 116, 609-614.

Zhang, H., Cai, C., Hu, Y., Jin, J., Wu, P. 2010. Graphene–gold nanostructure composites fabricated by electrodeposition and their electrocatalytic activity toward the oxygen reduction and glucose oxidation. *Electrochimica Acta* 56, 491–500.

Zhou, Y., et al. 2011. Detection of nodularin based on a monoclonal antibody in water and aquatic fish samples. *Food Control* 22, 797-800.

Zilberg, B. 1966. Gastroenteritis in Salisbury European children - a five-year study. *Cent. Afr. J. Med* 12(9), 164-168.